HHS Public Access

Author manuscript

Nat Cell Biol. Author manuscript; available in PMC 2023 February 01.

Published in final edited form as:

Nat Cell Biol. 2022 August ; 24(8): 1202–1210. doi:10.1038/s41556-022-00959-z.

ADAR1 downregulation by autophagy drives senescence independently of RNA editing by enhancing p16^{INK4a} levels

Xue Hao[1], **Yusuke Shiromoto**[2,#], **Masayuki Sakurai**[2,$], **Martina Towers**[1], **Qiang Zhang**[2], **Shuai Wu**[2], **Aaron Havas**[3], **Lu Wang**[4,5], **Shelley Berger**[4,5], **Peter D. Adams**[3], **Bin Tian**[2], **Kazuko Nishikura**[2], **Andrew V. Kossenkov**[2], **Pingyu Liu**[1,&,*], **Rugang Zhang**[1,*]

[1]Immunology, Microenvironment and Metastasis Program, The Wistar Institute, Philadelphia, PA, USA

[2]Gene Expression and Regulation Program, The Wistar Institute, Philadelphia, PA, USA

[3]Sanford Burnham Prebys Medical Discovery Institute, San Diego, CA, USA

[4]Penn Epigenetics Institute, Perelman School of Medicine, University of Pennsylvania, Philadelphia, PA, USA

[5]Department of Cell and Developmental Biology, Perelman School of Medicine, University of Pennsylvania, Philadelphia, PA, USA

Abstract

Cellular senescence plays a causal role in ageing and, in mice, depletion of p16^{INK4a}-expressing senescent cells delays ageing-associated disorders [1,2]. Adenosine deaminases acting on RNA (ADARs) are RNA editing enzymes that are also implicated as important regulators of human ageing and ADAR inactivation causes age-associated pathologies such as neurodegeneration in model organisms [3,4]. However, the role, if any, of ADARs in cellular senescence is unknown. Here we show that ADAR1 is post-transcriptionally downregulated by autophagic degradation to promote senescence through upregulating p16^{INK4a}. The ADAR1 downregulation is sufficient to drive senescence in both *in vitro* and *in vivo* models. Senescence induced by ADAR1 downregulation is p16^{INK4a} dependent and is independent of its RNA editing function. Mechanistically, ADAR1 promotes SIRT1 expression by affecting its RNA stability through HuR, an RNA binding protein that increases the half-life and steady state levels of its target mRNAs. SIRT1, in turn, antagonizes translation of mRNA encoding p16^{INK4a}. Hence, downregulation of

[*]**Corresponding author:** Rugang Zhang, Ph.D. rzhang@wistar.org, Or, Pingyu Liu, Ph.D. pingyu_liu@fudan.edu.cn.
[#]Present address: Department of Molecular Genetics, Graduate School of Medicine Kyoto University, Kyoto, Japan
[$]Present address: Research Institute for Biomedical Sciences, Tokyo University of Science, Chiba, Japan
[&]Present address: Human Phenome Institute, Zhangjiang Fudan International Innovation Center, Fudan University, Shanghai, China

Author contributions

H.X., P.L. and R.Z. designed the experiments. X.H., M.T., Q.Z., S.W. and P.L. performed the experiments and analysed data. A.V.K. performed the bioinformatic analysis. Y.S. and M.S. contributed to study design. L.W. and A.H. contributed key experimental materials and design. X.H., L.W., P.D.A., K.N., S.L.B., P.L., A.V.K and R.Z. wrote the manuscript. P.D.A., S.L.B., B.T., K.N., P.L. and R.Z. supervised studies. R.Z. conceived the study.

Competing Interests Statement

The authors have no financial and non-financial competing interests.

Code availability

The software and algorithms for data analyses used in this study are all well-established from previous work and are referenced throughout the manuscript.

ADAR1 and SIRT1 mediates p16^{INK4a} upregulation by enhancing its mRNA translation. Finally, Adar1 is downregulated during ageing of mouse tissues such as brain, ovary, and intestine, and Adar1 expression correlates with Sirt1 expression in these tissues in mice. Together, our study reveals an RNA-editing independent role of ADAR1 in regulating senescence by post-transcriptionally controlling p16^{INK4a} expression.

Cellular senescence is a state of stable growth arrest triggered by a number of stress inducers such as activation of oncogenes, short telomeres caused by extensive passaging and chemotherapeutics [5]. Senescence is implicated in tissue ageing and various physiological processes [6]. Senescence-associated growth arrest is mediated by activation of the p16^{INK4a}/pRb and/or p53/p21 tumor suppressive pathways [5]. For example, p16^{INK4a} expression increases with ageing in several mouse and human tissues and p16^{INK4a} promotes ageing by limiting proliferation and self-renewal [1]. Indeed, clearance of p16^{INK4a}-positive senescent cells delays ageing-associated disorders [2,7].

Adenosine deaminases acting on RNA (ADARs) convert adenosine to inosine in double-stranded RNA [8]. Three ADAR encoding genes are present in vertebrates, ADAR1, ADAR2 and ADAR3 [9]. ADAR1 is ubiquitously expressed, whereas ADAR2 is most highly expressed in the brain and ADAR3 expression is restricted to the brain [9]. ADAR1 has two isoforms, a full-length interferon-inducible ADAR1p150 and the constitutively expressed N-terminal truncated ADAR1p110 [9]. Additionally, ADAR1p110 shuttles between nucleus and cytoplasm in a p38 kinase dependent manner to promote survival of stressed cells [10]. Deletion of the single *Adar* gene in *Drosophila* causes age-dependent phenotypes such as neurodegeneration, which can be rescued by the catalytically inactive Adar mutant [3]. Defects in neurodegeneration of Adar mutant flies is linked to deregulation in autophagy pathway [11]. Further, inactivation of adr-1 and adr-2 in *C. elegans* reduces lifespan [4]. Finally, single nucleotide polymorphisms in ADARs are associated with extreme old age in humans [4].

Given the role of ADARs in regulating ageing and the contribution of senescence to tissue ageing, we examined the expression of ADAR1 in proliferating and replicative senescent (RS) human embryonic fibroblasts IMR90 cells. Both ADAR1p110 and ADAR1p150 isoforms were downregulated in RS cells (Fig. 1a). In contrast, there was no decrease in ADAR1 expression in quiescent cells (Extended Data Fig. 1a). Notably, we cannot detect ADAR2 expression in IMR90 cells (Extended Data Fig. 1b). Similar ADAR1 downregulation was also observed in both oncogenic H-RAS^{G12V} and etoposide-induced senescent cells (Fig. 1b and Extended Data Fig. 1c). To determine whether ADAR1 downregulation is sufficient to induce senescence, we knocked down ADAR1 using two independent short hairpin RNAs (shRNAs). ADAR1 knockdown induced expression of markers of senescence such as SA-β-Gal activity and a suppression of cell growth (Fig. 1c–e). Similar findings were also made by CRISPR-mediated ADAR1 knockout (Extended Data Fig. 1d–h). Notably, ectopic expression of either ADAR1p150 or ADAR1p110 suppressed the induction of SA-β-Gal activity induced by endogenous ADAR1 knockdown (Fig. 1f–g). This is consistent with the finding that both ADAR1p150 and ADAR1p110 are downregulated during senescence. Similarly, mouse embryonic fibroblasts isolated from

Adar1 knockout mice showed a significant increase in SA-β-Gal activity (Extended Data Fig. 1i–j). Likewise, acutely knocking down *Adar1* through hydrodynamic tail-vein injection triggered expression of SA-β-Gal activity in mouse hepatocytes (Fig. 1h–i and Extended Data Fig. 1k–m). Notably, Adar1 is downregulated in NRas-expressing hepatocytes *in vivo* (Fig. 1j–k). Together, we conclude that ADAR1 downregulation promotes senescence both *in vitro* and in mouse models.

ADAR1 mRNA expression was not downregulated during senescence (Extended Data Fig. 1n–o), indicating that ADAR1 downregulation occurs post-transcriptionally. Indeed, treating senescent cells with Lys05, an inhibitor of the autophagy-lysosome pathway [12], rescued ADAR1 protein downregulation in senescent cells (Fig. 2a and Extended Data Fig. 2a–b). Likewise, lysosome inhibitor Leupeptin partially rescued ADAR1 downregulation (Extended Data Fig. 2c–d). Lys05 does not affect ADAR1 expression in proliferating cells (Extended Data Fig. 2e), indicating that ADAR1 downregulation occurs only in autophagy-activated senescent cells [13,14]. Knocking down ATG7, an upstream autophagy regulator, impaired ADAR1 downregulation in RAS-induced senescent cells (Extended Data Fig. 2f–g). Similar observations were also made in RS of both IMR90 and WI38 cells (Extended Data Fig. 2h–k).

We next determined whether ADAR1 is an autophagy substrate during senescence. We observed a co-localization between LC3 and ADAR1 puncta in the cytoplasm of senescent cells (Extended Data Fig. 2l–m). The interaction between ADAR1 and LC3 was enhanced in senescent cells based on co-immunoprecipitation analysis (Fig. 2b and Extended Data Fig. 2n). Indeed, two LC3-interacting region (LIR) motif ADAR1 mutants that are deficient in LC3 binding also impaired its downregulation in senescent cells (Fig. 2c–e). We next used an mCherry-GFP-ADAR1p110 construct in which GFP is sensitive to low pH and mCherry-only signals of the tandem-tagged protein represents localization within acidic autolysosomes/lysosomes [14,15]. mCherry-GFP-ADAR1p110 showed predominantly nuclear localization in proliferating cells, whereas senescent cells showed cytoplasmic mCherry-only ADAR1p110 puncta that co-localized with lysosomal marker LAMP1 (Fig. 2f–g).

We observed that ADAR1p110, but not ADAR1p150, was exported from nucleus to cytoplasm in senescent cells (Fig. 2h–i and Extended Data Fig. 2o). Inhibition of ADAR1p110's nucleus export by p38 inhibitor SB203580 [10], but not MG132, an inhibitor of ubiquitin-mediated protein degradation, rescued the ADAR1p110 downregulation in senescent cells (Fig. 2j–k). These data support that the autophagy-lysosome pathway and ADAR1p110 nuclear export contribute to ADAR1 downregulation during senescence.

We next examined expression of $p16^{INK4a}$, p21 and p53 in ADAR1 knockdown cells. $p16^{INK4a}$, but not p21 and p53, is upregulated by ADAR1 knockdown or knockout (Fig. 3a–b). Senescence induced by $p16^{INK4a}$ upregulation is linked to heterochromatin formation [16]. Indeed, ADAR1 knockdown or knockout upregulated heterochromatic markers such as H3K27me3, H3K9me3 and HP1γ (Fig. 3a–b). Consistently, Adar1 knockdown correlated with an increase in H3K9me2 levels in mouse hepatocytes *in vivo* (Fig. 3c–d). Heterochromatin formation in senescent cells is mediated by the activation of the HIRA and PML body pathway [17]. Notably, ADAR1 knockdown or knockout significantly increased

the colocalization of HIRA and PML bodies (Fig. 3e–f), which correlated with an increase in the formation of senescence-associated heterochromatin foci (SAHF) as determined by macroH2A foci formation (Fig. 3g–h and Extended Data Fig. 3a). Lys05 treatment or ATG7 knockdown impaired SAHF formation (Fig. 3i–l and Extended Data Fig. 3b–c). We profiled changes in RNA expression induced by ADAR1 knockdown. A decrease in RNA editing induced by ADAR1 knockdown was confirmed in the RNA-seq analysis (Extended Data Fig. 3d). The RNA-seq and antibody array analysis revealed that ADAR1 knockdown did not induce a robust change in senescence-associated secretory phenotype (SASP) (Extended Data Fig. 3e–f). Known SASP regulators such as p65 NFκb and p38 MAPK were not altered by ADAR1 knockdown or knockout (Extended Data Fig. 3g–h). Further, SASP containing conditioned-media collected from OIS cells failed to further increase SA-β-Gal positive cells in ADAR1 knockdown cells (Extended Data Fig. 3i–j). These results suggest that senescence induced by ADAR1 knockdown is independent of the SASP. We conclude that ADAR1 downregulation promotes $p16^{INK4a}$ expression and the associated heterochromatin to induce senescence.

To determine whether senescence induced by ADAR1 downregulation depends on its RNA editing activity, we performed the rescue experiment in ADAR1 knockdown cells by either wildtype ADAR1 or a E912A ADAR1 mutant that is defective in RNA editing function [18]. Both wildtype and mutant ADAR1 rescued the expression of senescence markers including $p16^{INK4a}$ (Fig. 3m and Extended data Fig. 3k–m). These data support that ADAR1 regulates $p16^{INK4a}$ expression and senescence independent of its RNA editing function.

To determine whether $p16^{INK4a}$ and its regulated pRB are necessary for senescence induced by ADAR1 downregulation, we knocked down $p16^{INK4a}$ or pRB in ADAR1 knockdown cells (Fig. 4a–b). Knockdown of either $p16^{INK4a}$ or pRB is sufficient to overcome senescence induced by ADAR1 knockdown (Fig. 4c–e). We next determined the mechanism by which ADAR1 downregulation upregulates $p16^{INK4a}$. $p16^{INK4a}$ is transcriptionally regulated during senescence [19]. However, our RNA-seq analysis showed that $p16^{INK4a}$ mRNA was not induced by ADAR1 knockdown, which we validated by qRT-PCR analysis (Extended Data Fig. 4a). We next focused on changes in $p16^{INK4a}$ regulators in our RNA-seq analysis and focused on the downregulation of *SIRT1* induced by ADAR1 knockdown (Extended Data Fig. 4b). This is because SIRT1 is a known regulator of tissue ageing and is implicated in regulating $p16^{INK4a}$ at the translational level [20,21]. We validated downregulation of *SIRT1* mRNA induced by ADAR1 knockdown at both mRNA and protein levels (Fig. 4f and Extended Data Fig. 4c). Rescue of ADAR1 expression by p38 inhibitor, Leupeptin, Lys05 or shATG7 correlated with an increase in SIRT1 expression (e.g., Fig. 2j and Extended Data Fig. 2). Notably, ectopic SIRT1 expression overcomed senescence induced by ADAR1 knockdown (Fig. 4g–j). Consistently, ectopic SIRT1 suppressed the upregulation of $p16^{INK4a}$ induced by ADAR1 knockdown (Fig. 4g). We conclude that $p16^{INK4a}$ mediates senescence induced by ADAR1 downregulation through SIRT1 downregulation.

There is evidence to suggest that ADAR1 forms a complex with human antigen R (HuR), an RNA stability regulator whose association with its RNA targets depends on the presence of ADAR1 [22,23]. To determine whether ADAR1 affects the association of

HuR with *SIRT1* mRNA, we performed RNA immunoprecipitation using an anti-HuR antibody followed by sequencing. The analysis revealed that *SIRT1* mRNA was among the genes whose association with HuR was decreased by ADAR1 knockdown (Extended Data Fig. 4d and Supplementary Table 1). HuR knockdown activated autophagy as indicated by downregulation of p62 [24], which correlated with a reduction in ADAR1 expression (Extended Data Fig. 4e–f). We validated that ADAR1 knockdown significantly decreased the association of HuR with *SIRT1* mRNA (Fig. 4k). This correlates with a decrease in *SIRT1* mRNA stability in ADAR1 knockdown cells (Fig. 4l). Lys05 treatment or ATG7 knockdown rescued the observed decrease of HuR's association with *SIRT1* mRNA (Fig. 4m and Extended Data Fig. 4g). However, ADAR1 knockdown did not downregulate HuR expression (Extended Data Fig. 4h). Additionally, ADAR1 knockdown significantly increased the association of translation initiation factor EIF3a with $p16^{INK4a}$ mRNA (Fig. 4n), which correlated with an increase in $p16^{INK4a}$ mRNA translation as determined by polysome profile (Fig. 4o). Further, ATG7 knockdown partially rescued the downregulation of SIRT1 and upregulation of $p16^{INK4a}$ in replicative senescent IMR90 and WI38 cells (Extended Data Fig. 1h and 1j). We conclude that ADAR1 downregulation promotes senescence through upregulating $p16^{INK4a}$ at the translational level via destabilizing *SIRT1* mRNA due to a decrease in HuR binding (Fig. 4p).

To explore whether ADAR1 and its regulated SIRT1 are regulated during tissue ageing, we analyzed ADAR1 protein expression by immunoblot in three types of tissues obtained from young vs. aged mice. Adar1 is highly expressed in brain cortex, ovary and intestine tissues and its expression is downregulated in aged compared with young mice, which correlated with downregulation of Sirt1 (Extended Data Fig. 5a). Given that deletion of *Adar* gene in *Drosophila* causes age-dependent phenotypes such as neurodegeneration [3], we expanded the analysis into additional brain cortex tissues obtained from young and aged mice. ADAR1 protein levels were significantly decreased in aged compared with young mice (Fig. 5a–b). Consistently, Sirt1 was expressed at a significantly lower level in aged compared with young mice (Fig. 5c). Indeed, there is a positive correlation between Adar1 and Sirt1 expression in these brain tissues (Fig. 5d). In contrast to Adar1, expression of Adar2 and Adar3, both of which are highly expressed in brain tissues [9], are not regulated during tissue ageing (Fig. 5a and Extended Data Fig. 5b–c). We were unable to obtain a $p16^{INK4a}$ antibody that can detect mouse $p16^{INK4a}$ protein expression. Likewise, Adar1 was expressed at a significantly lower level in aged mouse ovary tissues compared with those observed in young mice (Fig. 5e–f). To determine whether inhibition of autophagy impairs the age-associated downregulation of ADAR1, we examined Adar1 expression in ovary of young and aged mice treated with vehicle PBS or Lys05. Indeed, Lys05 treatment significantly increased Adar1 expression in aged mouse ovary tissues (Fig. 5e–f). There was a significant downregulation of Sirt1 in aged compared with young mouse ovary (Fig. 5g). Consistently, Lys05 treatment significantly increased Sirt1 expression in aged mouse ovary tissues (Fig. 5g). In addition, there was a positive correlation between Adar1 and Sirt1 expression in these ovary tissues (Fig. 5h). Similar findings were also made in young, aged and Lys05 treated aged mouse intestine tissues (Extended Data Fig. 5d–g). However, *Adar1* mRNA was not significantly downregulated in aged mouse ovary or intestine tissues compared with young tissues (Extended Data Fig. 5h–i). Indeed, Lys05 treatment increased p62 levels in

aged mouse ovary and intestine tissues (Extended Data Fig. 5j–m). We conclude that Adar1 is downregulated during ageing and its expression correlates with Sirt1 expression in mouse brain, ovary and intestine tissues.

The $p16^{INK4a}$ expression is one of the best ageing biomarkers [19]. In addition, $p16^{INK4a}$ is a key effector of cellular senescence that contributes to tissue ageing [19]. $p16^{INK4a}$ is not simply a passive biomarker of organism ageing because inducible elimination of $p16^{INK4a}$ positive cells delays/attenuates age-associated disorders [1,2,7]. Thus, understanding how $p16^{INK4a}$ expression is regulated during senescence and ageing is of high significance. Previous studies have established several transcription factors and epigenetic regulators that function as effectors of signaling pathways to regulate $p16^{INK4a}$ expression during senescence and ageing [19]. However, these regulations occur at the transcriptional levels in senescent cells [19]. Our results demonstrated that $p16^{INK4a}$ is regulated at the translational level downstream of ADAR1 controlled SIRT1 translation during senescence. Further studies are warranted to investigate the relative contribution of transcriptional and translational control to $p16^{INK4a}$ upregulation during organism ageing.

Autophagy is a lysosomal degradation pathway that supports the clearance of protein aggregates and damaged subcellular structure to maintain homeostasis [25]. Autophagy increases the lifespan of model organisms and increased basal autophagy prevents premature ageing, improves health span and promotes longevity in mouse models [26]. Our studies indicate that autophagy may promote tissue ageing by activating the ADAR1-SIRT1-$p16^{INK4a}$ pathway. This is consistent with previous studies that autophagy mediates the degradation of lamin B1 and SIRT1 to drive senescence [13,14]. Thus, autophagy plays a context-dependent role in tissue ageing and inhibition of autophagy may be explored as a way to regulate senescence. Notably, in addition to subjecting to direct autophagy-mediated degradation during ageing in tissues such as spleens, testes and thymus [14], our findings suggest that *SIRT1* is regulated at the mRNA stability level as a consequence of autophagy-mediated ADAR1 downregulation in tissues such as brain, ovary and intestine. Reactivating SIRT1 function has been proposed as a critical means to combat tissue ageing [27–29]. Indeed, SIRT1 ectopic expression is sufficient to overcome senescence induced by ADAR1 downregulation. Thus, inhibition of autophagy appears to be an attractive strategy to restore SIRT1 levels in aged tissue.

Genetic studies in model organism clearly established a role of ADARs in regulating life span and age-associated disorders [3,4]. Adar knockout in *Drosophila* causes defects in normal locomotion and age-dependent neurodegeneration [3]. Interestingly, a catalytically inactive protein is sufficient to rescue neurodegeneration in *Adar* mutants [3]. Consistently, senescence induced by ADAR1 downregulation is independent of its RNA editing function and we observed a decrease of ADAR1 expression in brain tissues obtained from aged mice compared with those from young mice. In addition, ADAR1 downregulation can be restored by autophagy inhibition. This raises the possibility to inhibit the autophagy pathway as a critical means to restore ADAR1 expression in aged tissues such as brain, which may prevent age-associated neurodegeneration. In summary, our findings provide a mechanistic link between ADAR1 and organism ageing by revealing that ADAR1 downregulation

promotes senescence through translationally upregulating $p16^{INK4a}$ expression in an RNA-editing independent manner.

Methods

Cells and culture conditions

IMR90 and WI38 fibroblasts were cultured under 2% O_2 in DMEM medium supplemented with 10% fetal bovine serum (FBS), glutamine, sodium pyruvate, non-essential amino acids and sodium bicarbonate. PD30 IMR90 cells were used unless otherwise stated. The 293FT, Phoenix and mouse ID8 cells were cultured in DMEM medium with 10% FBS and 1% penicillin–streptomycin under 5% CO_2. All of the cell lines were authenticated at The Wistar Institute's Genomics Facility using short-tandem-repeat DNA profiling. Regular mycoplasma testing was performed using the LookOut mycoplasma PCR detection kit (Sigma, cat. no. MP0035).

Retrovirus and lentivirus production and infection

Retrovirus was produced using Phoenix cells as previously described [17]. Lentivirus was produced in 293FT cells with packaging plasmids using Lipofectamine 2000 (Thermo Fisher, cat. no. 11668019) based on the manufacturer's instructions. IMR90 fibroblasts infected with viruses encoding the puromycin resistance gene were selected using puromycin (1 μg ml^{-1}).

Colony-formation assay

Cells were seeded in six-well plates at a density of 3,000 cells per well and cultured for 10 days before staining with 0.05% crystal violet for visualization. Analysis was performed based on integrated density using the NIH ImageJ (1.48v).

RNA-sequencing

IMR90 cells were harvested, and the RNA was extracted using RNeasy mini Kit (Qiagen, cat. no. 74106) and digested with DNase I (Qiagen, cat. no. 79254). The libraries were prepared using a KAPA RNA HyperPrep kit (Roche, cat. no: 07962312001) and sequenced in a 75-bp paired-end run at the Wistar Genomics Facility using an Illumina NextSeq 500 system.

Reverse-transcriptase qPCR (RT-qPCR)

Extracted RNA was used for reverse-transcriptase PCR using a High-capacity cDNA reverse transcription kit (Thermo Fisher, cat. no. 4368814). Quantitative PCR was performed using a QuantStudio 3 real-time PCR system. The primers used for reverse-transcriptase qPCR are listed in Supplementary Table 2.

Reagents, plasmids, and antibodies

Etoposide was purchased from Sigma (cat. no. E1383, 100 μM for 48h). Lys05 was purchased from Selleck (cat. no. S8369, 5 μM for 48h). SB203580 was purchased from Selleck (cat. no. S1076, 10 μM for 48h), MG132 was purchased from Selleck (cat. no.

S2619, 0.5 μM for 48h). Leupeptin was purchased from Sigma (cat. no. EI8, 10 μg/ml for 48h). BAY 11-7082 was purchased from MedChemExpress (cat. no. HY-13453, 5 μM for 48h). Actinomycin D was purchased from Thermo Fisher (cat.no. 11805017, 5 μg/mL).

The shRNAs against the following human genes were obtained from the Molecular Screening Facility at the Wistar Institute: shADAR1 #1, TRCN0000050788; shADAR1 #2, TRCN0000050789; shp16, TRCN0000010482; shRB, TRCN0000010419; shAtg7, TRCN0000007584; shHuR #1, TRCN0000017274, shHuR #2, TRCN0000017277. pLKO.1-puro -CMV-TurboGFP shRNA Control plasmid was purchased from Sigma (cat. no. SHC003), the shRNAs against mouse *Adar1* was purchased from Sigma (cat. no. TRCN0000218395) with CMV-TurboGFP. sgRNAs were cloned into LentiCRISPR v2 (Addgene #52961) linearized with BsmBI. The oligonucleotides used for sgRNAs are listed in Supplementary Table 2. The Transposon-based plasmid pKT2-NRas^{V12}-DsRed2-miR-30-shRenilla-Luciferase and pPGK-Transpose plasmids were generated as previously described [30].

mCherry-ADAR1p110/p150 and wildtype and enzymatic mutant ADAR p110 E912A plasmid were gifts of Dr. Kazuko Nishikura and subcloned into the pCDH vector by using the Spe1 and BamH1 restriction enzyme sites. pBabe-mCherry-GFP-construct was a gift of Dr. Shelley Berger and ADAR1p110/p150 sequences were cloned into the construct. Site-specific mutations of ADAR1p110 were generated using Q5 Hot Start HiFi PCR Master Mix (New England Biolabs) according to the manufacturer's instruction. Primers used for ADAR1p110 mutations are listed in Supplementary Table 2. All mutation sites were confirmed by Sanger sequencing at The Wistar Institute's Genomics Facility.

The following antibodies were purchased from the indicated suppliers. For western blots: mouse anti-ADAR1 (Santa Cruz Biotechnology, cat. no. SC-73408; 1:200), mouse anti-ADAR2 (Santa Cruz Biotechnology, cat. no. SC-73409; 1:1000), rabbit anti-ADAR3 (Novus, NBP1-57558, 1:1000), rabbit anti-SIRT1 (Millipore, cat. no. 07-131; 1:1000), rabbit anti-HuR (Cell Signaling Technology, cat. no. 12582; 1:1000), mouse anti-p16^{INK4a} (Abcam, cat. no. ab16123, 1:500), mouse anti-p21 (Abcam, cat. no. 7901; 1:1000), mouse anti-p53 (Calbiochem, cat. no. OP43; 1:1000), rabbit anti-HP1γ (Cell Signaling Technology, cat. no. 2619, 1:1000), rabbit anti-H3K27me3 (Cell Signaling Technology, cat. no. 9733, 1:1000), rabbit anti-H3K9me3 (Abcam, cat. no. ab8898, 1:1000), mouse anti-p62 (Cell signaling Technology, cat. no. 88588, 1:1000), rabbit anti-ATG7 (Cell signaling Technology, cat.no. 8558T, 1:1000), mouse anti-RAS (BD Biosciences, cat. no. 610001; 1:1000), mouse anti-LC3β (Santa Cruz, cat. no. sc-376404, 1:200), mouse anti-V5 (Invitrogen, cat. no. MA5-15253, 1:1000), rabbit anti-GAPDH (Cell Signaling Technology, cat. no. 5174S, 1:3000), mouse anti-β-actin (Sigma, cat. no. A1978, 1:5000). For immunofluorescence, mouse anti-HIRA (WC119/WC19/WC117 from Adams Lab; 1:100 as previously published [31]), rabbit anti-macroH2A1.2 (#70288 from Adams Lab; 1 μg ml^{-1} as previously published [31]), mouse anti-PML (Chemicon, cat. no. AB1370; 1:1000), rabbit anti-γH2AX (Millipore, cat. no. 07-131; 1:100), rabbit anti-NRas (Proteintech, cat. no. 10724-1-AP; 1:100), mouse anti-ADAR1 (Santa Cruz Biotechnology, cat. no. SC-73408, 1:50), mouse anti-GFP (Invitrogen, cat. no. MA5-15256, 1:200), rabbit anti-H3K9me2 (Cell Signaling Technology, cat. no. 4658, 1:200), rabbit anti-LAMP1 (Cell Signaling Technology, cat. no. 9091T,

1:100) and rabbit anti-LC3β (Cell Signaling Technology, cat. no. 3868S, 1:500). Alexa fluor secondary antibodies: Alexa Fluor™ 488 goat anti-mouse IgG (Invitrogen, cat. no. A-10680, 1:400), Alexa Fluor™ 647 donkey anti-mouse IgG (Invitrogen, cat. no. A-32787, 1:400), Alexa Fluor™ 488 goat anti-rabbit IgG (Invitrogen, cat. no. A-11008, 1:400). For immunoprecipitation: rabbit anti-ADAR1 (Sigma, cat. no. HPA003890; 1:40) and rabbit anti-EIF3a (Cell Signaling Technology, cat. no. 3411; 1:100).

Antibody array analysis

The antibody array for secreted factors was performed using a Human Cytokine Antibody Array C3 (RayBiotech, cat. no. AAH-CYT-3-4) based on the manufacturer's instructions. Briefly, conditioned medium was generated from cells following a PBS wash and incubation in serum-free DMEM for 48 hrs. Conditioned medium was filtered (0.2 μm) and incubated on the array overnight at 4 °C. Following incubation, the array was washed three times with Wash Buffer I and then twice with Wash Buffer II at room temperature. The array was then incubated with the biotinylated antibody cocktail for 2 hrs at room temperature before being washed three times with Wash Buffer I and then twice with Wash Buffer II at room temperature. The array was then incubated with HRP-streptavidin and incubated for 2 hrs at room temperature. Following incubation, the array was washed three times with Wash Buffer I and then washed twice with Wash Buffer II. The membrane was then incubated with Detection Buffer mixture for 2 minutes at room temperature, the signals were then measured using Konica Medical Film Processor Model SRX-101A and quantified with NIH ImageJ software (1.48v) followed by normalization to the cell number from which the conditioned medium was generated.

Quiescence induction

Cellular quiescence was induced following the description with some modifications [32]. Specifically, cells were cultured in normal condition and changed to 0.1% FBS medium when confluency reached to ~80% for 7 days and then were harvested for analysis.

Senescence induction and SA-β-gal staining

For ER:RAS senescence induction [33], IMR90 cells were infected with lentivirus encoding a 4-hydroxy-tamoxifen (4-OHT) inducible ER:RAS construct (pLNC-ER:Ras), after two-weeks of selection with G418 (400 μg/ml, Gibco), cells were maintained with lower dose of G418 (200 μg/ml) and treated with 4-OHT at a final concentration of 100 nM, cells were harvested to examine the expression of RAS and other markers at indicated time points. Senescence induced by oncogenic H-RAS^{G12V} or treatment with Etoposide was performed as described [34]. Specifically, for SA-β-gal staining, cells were fixed using 2% formaldehyde and 0.2% glutaraldehyde in PBS and washed twice with PBS. The cells were then incubated overnight in X-gal solution (150 mM NaCl, 40mM Na_2HPO_4, pH6.0, 2mM $MgCl_2$, 5mM $K_3Fe(CN)_6$, 5mM $K_4Fe(CN)_6$ and 1mg ml^{-1} X-gal) at 37°C in a non-CO_2 incubator. For mouse liver tissue, frozen sections were fixed and stained at pH 5.5 for 5 – 8 hrs.

Immunoblotting and immunofluorescence

For immunoblotting, protein was isolated by lysing cells or tissues in 1 X sample buffer (10% glycerol, 2% SDS, 0.01% bromophenol blue, 0.1 M dithiothreitol and 62.5 mM Tris-HCl pH 6.8). Equal amounts of proteins were loaded and separated by SDS–PAGE and transferred to a polyvinylidene fluoride membrane (Millipore). The membranes were blocked with 5% non-fat milk in TBS/0.1% Tween 20 (TBST) for 1 hr at room temperature and then incubated with primary antibody at 4°C overnight in 4% BSA/TBS + 0.025% sodium azide. The next day, the membrane was washed with TBST for 10 min at room temperature and then incubated in HRP-conjugated secondary antibodies (Cell Signaling Technology). Following incubation with the secondary antibodies, the membrane was washed in TBST for 10 min at room temperature for four times and then incubated with SuperSignal West Pico PLUS Chemiluminescent Substrate (Thermo Fisher) for visualization on film.

For immunofluorescence staining, cells on coverslips or tissues from frozen section were fixed with 4% PFA for 15 min at room temperature. Cells/tissues were washed twice with PBS followed by permeabilization with 0.2% Triton X-100 in PBS for 20 min. After washing twice, cells/tissues were blocking with 1% BSA in PBS for 20 min at room temperature. Cells/tissues were incubated with primary antibody at 4°C overnight. The next day, cells/tissues were washed three times in PBS supplemented with 0.1% Tween 20 (PBST) and probed with Alexa Fluor-conjugated secondary antibody (Life Technologies) for 1 hr at room temperature. Cells/tissues were washed and subjected to 1 μg ml^{-1} 4,6-diamidino-2-phenylindole (DAPI) staining for 5 min at room temperature, after washing four time with PBST, the slides were sealed and imaged using a Leica TCS SP5 II scanning confocal microscope.

RNA immunoprecipitation (RIP) and qRT–PCR analysis

Anti-HuR RIP was performed as follows: for RNA-sequencing in IMR90 cells with or without ADAR1 knockdown, and HuR's association with *SIRT1* mRNA in control and senescent IMR90 cells with or without autophagy inhibition, RIP was carried out using a Magna RIP® RNA-Binding Protein Immunoprecipitation Kit (Millipore, cat. no. 17-700). Briefly, for each immunoprecipitation, 2×10^7 cells were harvested and lysed in 100 μl RIP Lysis Buffer with RNase and protease inhibitors. The lysate was subjected to immunoprecipitation using 5 μg anti-HuR antibody (Millipore, cat. no. 03-102). The immunoprecipitated RNAs were extracted using phenol : chloroform : isoamyl alcohol (Thermo Fisher, cat. no. AM9720) followed by quantitative PCR or RNA-seq. For validation RIPs, cDNA was synthesized using High-Capacity cDNA Reverse Transcription Kit (Thermo Fisher, cat. no. 4368814). Quantitative PCR primers are listed in the Supplementary Table 2. For the RNA-seq, the RNA library was prepared using KAPA RNA HyperPrep kit (Roche, cat. no. 07962312001). shHuR-expressing cells were used as a positive control.

For the RIP procedure for HuR's association with *SIRT1* mRNA [10], the cells were fixed with 0.1% formaldehyde in PBS at room temperature for 5 min. The cytoplasmic fraction was sonicated, and the lysate was incubated with antibody for overnight at 4 °C. The RNA–

protein complexes captured on beads were washed five times with high-salt buffer (50 mM Tris-HCl, pH 7.6, 1 M NaCl, 1% NP-40, 0.5% sodium deoxycholate, 0.1% SDS, and 1 mM EDTA), then with suspension buffer (50 mM Tris-HCl, pH 7.6, 150 mM NaCl, and 1% NP-40). The RNA was reverse-crosslink was performed [10] and purified with TRIzol LS (Thermo Fisher). RT–QPCR was performed with primers as listed in the Supplementary Table 2.

Polysome profiling

Polysome profiling was carried out as detailed below [35]. 3×10^7 cells were first washed with ice-cold PBS containing 100 mg/ml cycloheximide, then harvested and suspended in hypotonic buffer (10 mM HEPES, pH 7.9, 1.5 mM $MgCl_2$, 10 mM KCl, 200 U/ml SUPERaseIn RNase inhibitor, 1x protease inhibitor cocktail, and 0.5 mM DTT). Cells were put on ice for 10 min, then Dounce-homogenized for 10 times. Cell lysates were subjected to centrifugation at 14,000 × g for 10 min to remove the nuclear pellet. The supernatant was loaded onto a 10 mL 10%–50% sucrose gradient in a polyallomer tube containing 20 mM HEPES-KOH pH 7.5, 15 mM $MgCl_2$, 80 mM KCl, 2mM DTT, and 100 mg/ml cycloheximide followed by centrifugation in a TH-641 rotor (Thermo Fisher) at 19,000 g at 4 °C for 2 hr. The gradient was then fractionated using a system comprising a syringe pump (Harvard Apparatus model 11), a density gradient fractionator (Brandel), and an ISCO UA-6 UV/VIS detector. Each lysate was partitioned into ribosome-free, monosome, and polysome fractions based on UV absorbance. Monosome and polysome fractions were incubated with 25 mM EDTA (pH 8.0), 10 mM Tris-HCl (pH 7.0), and 1% SDS at 65 °C for 5 min, followed by extraction of RNA with phenol-chloroform and Ethanol precipitation.

Immunoprecipitation (IP)

For endogenous ADAR1-LC3 interaction detection, the cells were lysed in ice-cold lysis buffer containing 20 mM Tris pH 8.0, 137 mM NaCl, 1% NP-40 and 2 mM EDTA, supplemented with protease inhibitor cocktail (Roche, cat no. 4693116001) and maintained gentle rotation at 4 °C for 30 min. The supernatant was incubated with anti-ADAR1 antibody at 4 °C overnight, and then 20 μl protein A/G-coupled agarose beads were added, the lysate beads mixture was incubated at 4 °C under gentle rotation for 2 hr. The mixture was then put on a magnetic stand and washed three times before boiled with 2 x SDS loading buffer for western blot analysis. For detection of the interaction between ADAR1p110 wildtype/mutants and LC3, IP was performed using ChromoTek GFP-Trap Magnetic Particles M-270 (Proteintech, cat. no. gtd) according to the manufacturer's instruction.

RNA Stability Assay

RNA stability assay was performed as described [36]. Cells were treated with actinomycin D (5μg/mL) to inhibit RNA transcription and RNA was harvested at 0, 2, 4 or 6 hours post treatment. Total RNA was extracted by RNeasy mini Kit and used for RT-qPCR analysis.

Bioinformatic analysis

RNA-seq and HuR immunoprecipitation followed by sequencing data was aligned using *bowtie2* [37] against hg19 version of the human genome and *RSEM* v1.2.12 software [38] was used to estimate raw read counts and FPKM values using Ensemble transcriptome. For RNA-seq differential gene expression, *DESeq2* [39] was employed to normalize gene expression values and the values were used to calculate fold changes between conditions. FPKM and fold changes for selected genes were visualized in heatmaps. HuR immunoprecipitation pulldown fold changes were calculated vs. corresponding input sample and sample under HuR knockdown condition was additionally normalized to reduction fold change of HuR mRNA expression. Genes that were enriched in control pulldown sample vs. input experiment (at least 20%) that showed at least 20% reduction in the pulldown in both ADAR1 knockdown and HuR knockdown experiment that resulted in at least 1.5-fold reduction of mRNA expression (input) in both ADAR1 knockdown and HuR knockdown cells were reported. Varscan2 [40] was used to call putative A->I editing sites and overlapped with known SNPs using dbSNP 153 database. Sites that were not in a list of known SNPs covered with at least 10 reads and that showed at least 20% A->G substitution were considered as an A->I editing event.

In vivo mouse models

All of the protocols were approved by the IACUC of the Wistar Institute. Mice were maintained at 22–23°C with 40–60% humidity and a 12 h light - 12 h dark cycle.

For hydrodynamic tail-veil injection, eight-week-old female C56BL/6 mice were used. For each injection, endotoxin-free transposon-based construct expressing N-Ras^{G12V} (25 μg) together with endotoxin-free transposase plasmid (5 μg) were mixed or shRNAs (30 μg) in 0.9% saline at a volume of 10% of the mouse body weight were delivered into the mice within 5 – 8 seconds as previously described [41]. Mice were euthanized 6 days post injection, livers were collected and embedded in O.C.T. (Fisher, cat. no. 23-730-571) followed by flesh frozen.

For the Lys05 injection experiment, the aged mice (20 months) were obtained from National Institute on Aging-aged rodent colonies and were randomly grouped into two groups, injected intraperitoneally daily with 10 mg kg^{-1} Lys05 in PBS or PBS alone in a 100 μl volume for 2 weeks, then the mice were euthanized, and the tissues were harvested.

Statistical analysis

Experiments were repeated at least three times. All bar graphs show mean values with error bars (s.d. or s.e.m. as defined in figure legends). Analysis of variance with Fisher's least significant difference was used to identify significant differences in multiple comparisons. An unpaired two-tailed Student's *t*-test was used for comparison between two groups.

Extended Data

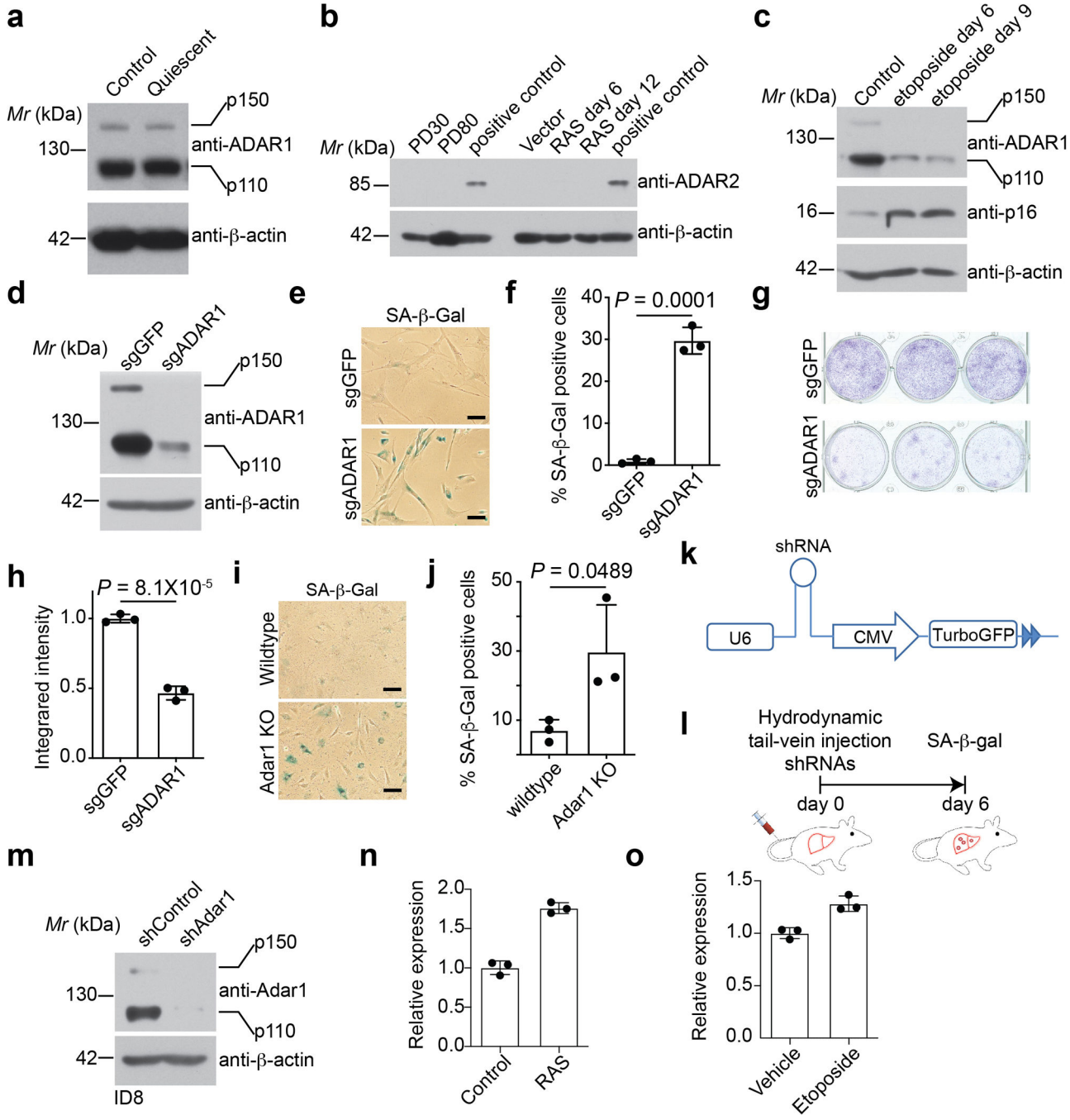

Extended Data Figure 1: ADAR1 downregulation during senescence

a, Expression of ADAR1 in the indicated control proliferating and quiescent IMR90 cells induced by contact inhibition and serum starvation was determined by immunoblot analysis. The experiment was repeated three times independently with similar results.

b, Expression of ADAR2 in control proliferating (PD30), replicative senescent (PD80), and RAS-induced senescent IMR90 cells was determined by immunoblot. Mouse brain tissue

was used as a positive control for ADAR2 expression. The experiment was repeated three times independently with similar results.

c, IMR90 cells were induced to senesce by Etoposide (100 μM for 48h) and examined for expression of the indicated proteins by immunoblot at the indicated point points. The experiment was repeated three times independently with similar results.

d-h, IMR90 cells expressing the indicated sgRNAs were analyzed for expression of the indicated proteins by immunoblot (**d**), or stained for SA-β-gal activity (**e**). Percentages of SA-β-Gal positive cells were quantified (from >200 cells) (**f**). The indicated cells were also subjected to colony formation assay to determine senescence-associated growth arrest (**g**), and the intensity of colony formed by the indicated cells was quantified by NIH ImageJ software (**h**). Scale bars = 100 μm.

i-j, Mouse embryonic fibroblasts isolated from wildtype control and Adar1 knockout mouse were stained for SA-β-Gal activity (**i**). Percentages of SA-β-Gal positive cells were quantified (from >200 cells) (**j**). Scale bars = 100 μm.

k-l, Schematic of the construct used to knock down Adar1 expression in mouse (**k**) and outline of hydrodynamic tail vein injection to induce senescence by Adar knockdown in mouse liver (**l**).

m, Validation of Adar1 knockdown in mouse cells. Mouse ID8 cells expressing the indicated shControl or shAdar1 were examined for expression of the indicated proteins.

n-o, *ADAR1* mRNA expression was determined by RT-qPCR analysis RAS-induced senescent IMR90 cells (**n**) or Etoposide induced senescent IMR90 cells (**o**).

Data represent the mean ± s.d. of three biologically independent experiments. *P* values were calculated using a two-tailed Student's *t*-test. Source numerical data and unprocessed blots are available in source data.

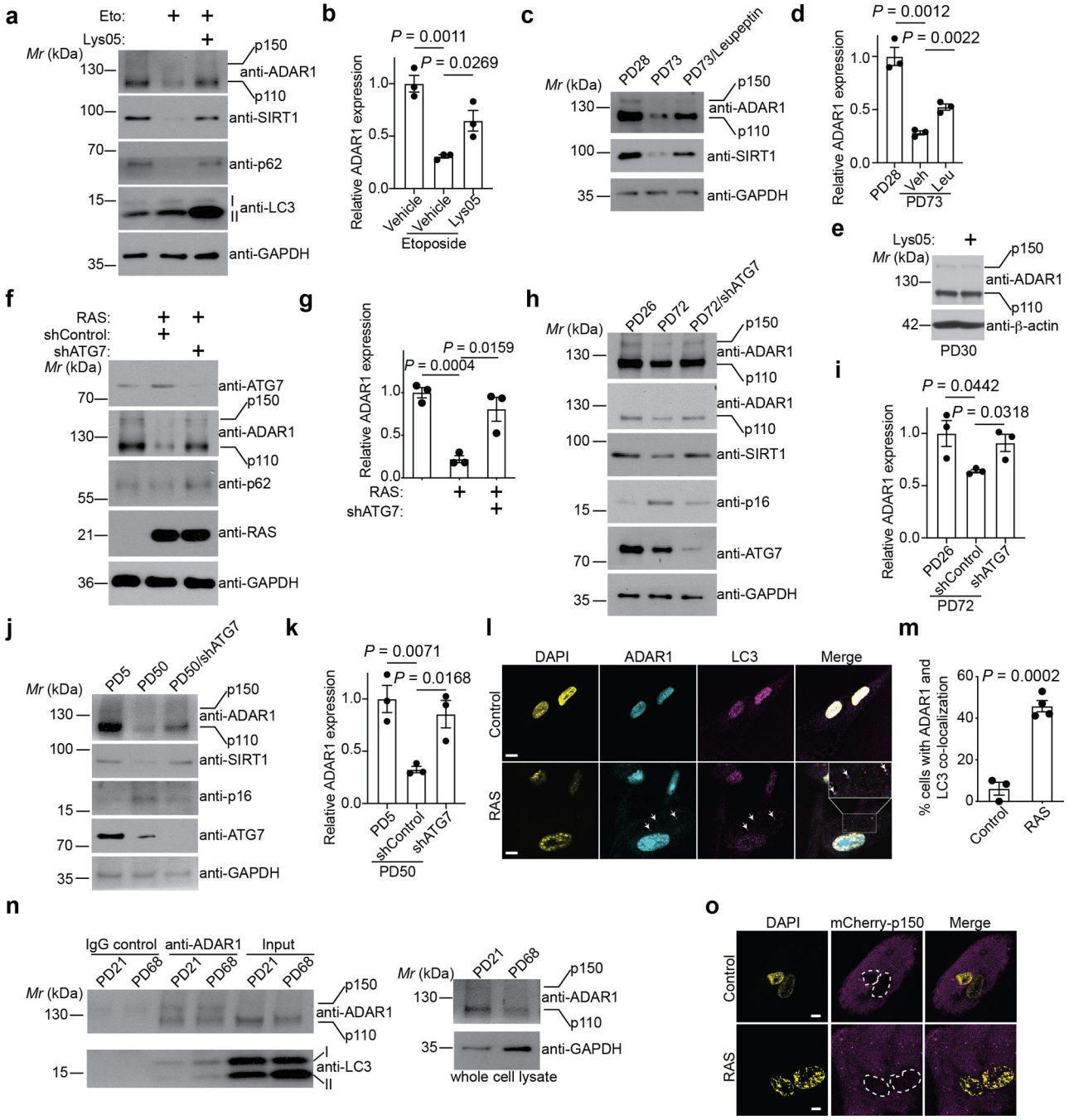

Extended Data Figure 2: Autophagy contributes to ADAR1 downregulation during senescence

a-b, Expression of the indicated proteins was determined by immunoblot in IMR90 cells treated with vehicle control or etoposide to induce senescence with or without simultaneous treatment of Lys05 (**a**) and relative ADAR1 levels were quantified (**b**). The experiment was repeated three times independently with similar results.

c-d, Expression of the indicated protein was determined by immunoblot in proliferating (PD28) and replicative senescent (PD73) IMR90 cells treated with or without Leupeptin (**c**)

and relative ADAR1 levels were quantified (**d**). The experiment was repeated three times independently with similar results.

e, Expression of the indicated proteins was determined by immunoblot in young and proliferative IMR90 (PD30) treated with or without Lys05 (**e**). The experiment was repeated three times independently with similar results.

f-g, Expression of the indicated proteins was determined by immunoblot in IMR90 cells induced to undergo senescence by oncogenic H-RAS^{G12V} with or without expressing shATG7 (**f**) and relative ADAR1 levels were quantified (**g**).

h-k, Expression of the indicated proteins was determined by immunoblot in control early passage proliferating or late passage replicative senescent IMR90 (**h**) or WI38 cells (**j**) with or without ATG7 knockdown. And relative ADAR1 levels were quantified in **i** and **k**.

l-m, Representative confocal images of immunostaining of endogenous ADAR1 and LC3 in control proliferating and RAS-induced senescent IMR90 (**l**). And the percentage of cells with co-localization of cytoplasmic ADAR1 puncta and LC3 (as exemplified by arrows pointed puncta) were quantified in 4 independent biological repeats (**m**).

n, Co-immunoprecipitation analysis between ADAR1 and LC3 in cytoplasmic extracts from the indicated proliferating (PD21) and replicative senescent (PD68) IMR90 cells. Downregulation of ADAR1 was validated in whole cell lysates.

o, IMR90 cells transfected with mCherry-ADAR1 p150 were induced senescence by expressing oncogenic H-RAS^{G12V}. Localization of mCherry-ADAR1p150 was visualized and DAPI counter staining was used to visualize nuclei. Scale bars = 10 μm.

Data represent the mean ± s.e.m. of three biologically independent experiments unless otherwise stated. *P* values were calculated using a two-tailed Student's *t*-test. Source numerical data and unprocessed blots are available in source data.

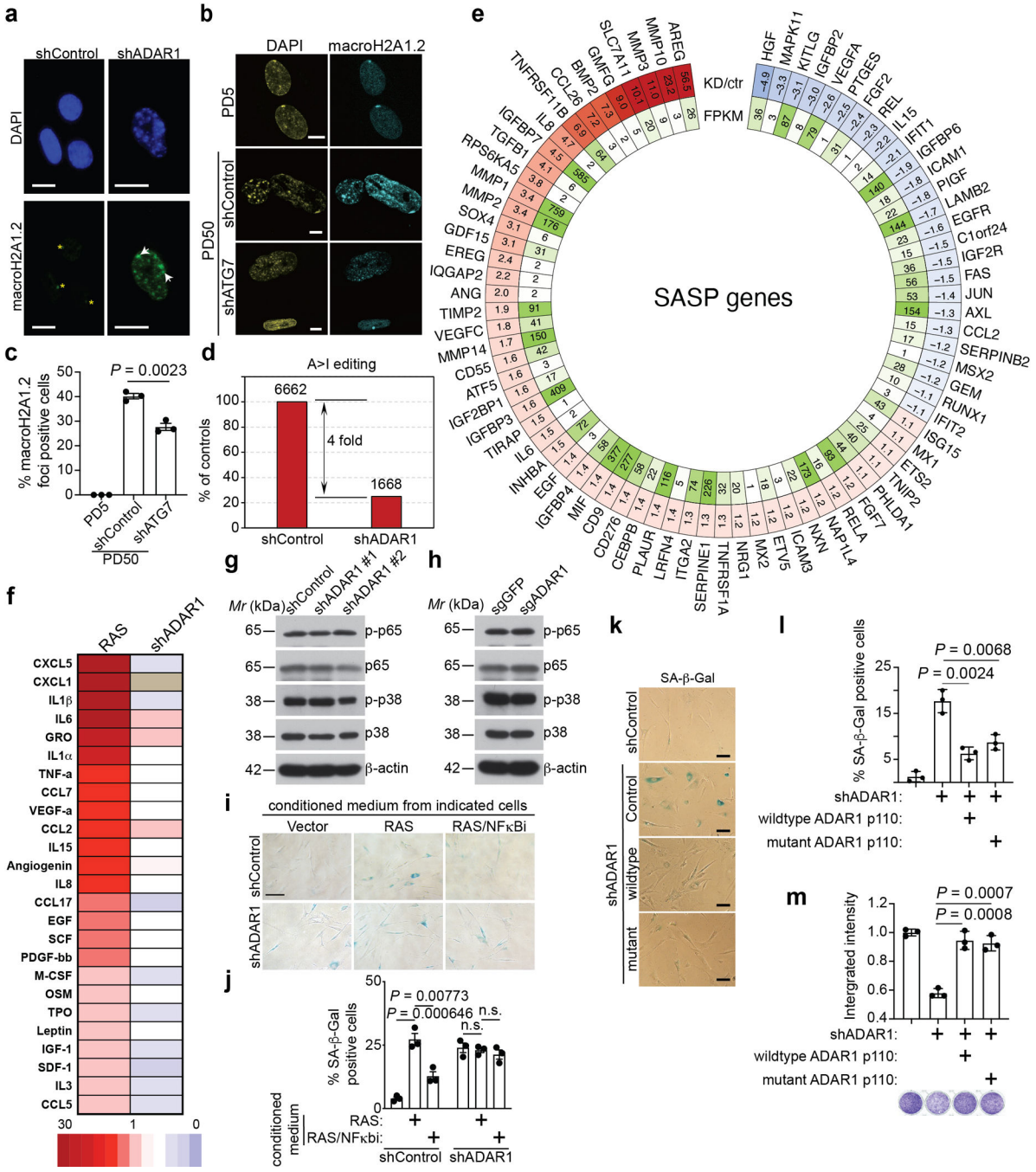

Extended Data Figure 3: ADAR1 downregulation does not induce robust SASP

a, Immunostaining for macroH2A1.2 in IMR90 cells with or without ADAR1 knockdown (shADAR1 #1). Scale bar = 10 μm. Asterisks indicated inactivated X chromosome in female IMR90 cells and arrows indicate examples of macroH2A1.2 positive SAHF. The experiment was repeated three times independently with similar results.

b-c, Immunostaining for macroH2A1.2 in control proliferating and replicative senescent WI38 cells with or without ATG7 knockdown (**b**). Cells with macroH2A1.2 positive foci were quantified (> 200 cells) (**c**). Scale bar = 10 μm.

d, Global RNA A/I editing was analyzed based on the RNA-seq A/G reads in the indicated cells.

e, Changes in expression of SASP genes in the indicated ADAR1 knockdown vs. control IMR90 cells (KD/Ctr) determined by RNA-seq analysis. SASP genes with at least 10 counts at least 1 FPKM level are reported.

f, Secreted cytokines in conditioned media from IMR90 cells with or without ADAR1 knockdown (shADAR1 #1) was detected using an antibody-based cytokine array. Conditioned media collected from RAS-induced senescent IMR90 cells was used as a positive control.

g-h, Expression of the indicated proteins was determined by immunoblot in IMR90 cells expressing shControl or shADAR1s (**g**) or sgGFP control or sgADAR1 (**h**). The experiment was repeated three times independently with similar results.

i-j, Representative images of SA-β-gal staining of IMR90 cells cultured with conditioned media from indicated cells (**i**). Percentages of SA-β-gal positive cells were quantified (from > 200 cells) (**j**).

k-m, IMR90 cells expressing shControl or shADAR1 (#1) with or without ectopically expression of wildtype ADAR1 p110 or a deaminase inactive mutant E912A ADAR1 p110 were analyzed for SA-β-Gal activity (**k**) and positive cells were quantified (from >200 cells) (**l**). In addition, the indicated cells were subjected to colony formation assay (**m**). Scale bars = 100 μm.

Data represent the mean ± s.d. in l and m, or s.e.m. in c and j of three biologically independent experiments. *P* values were calculated using a two-tailed Student's *t*-test. *P* values were calculated using a two-tailed Student's *t*-test. Source numerical data and unprocessed blots are available in source data.

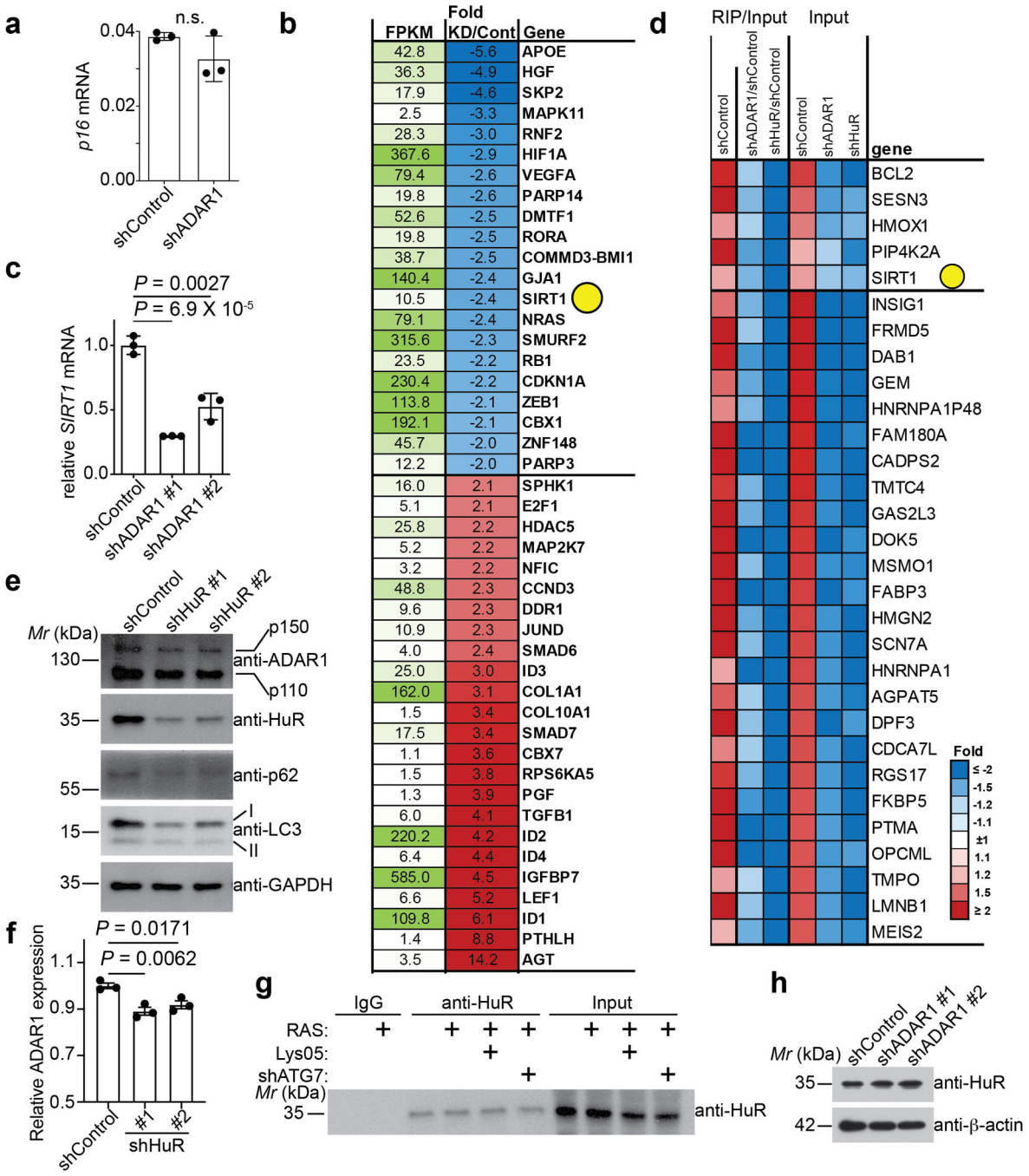

Extended Data Figure 4: ADAR1 regulates SIRT1 expression

a, Expression of *p16*^{INK4a} mRNA expression was analyzed by RT-qPCR in the indicated IMR90 cells.

b, Heatmap visualization of detected (at least 10 read counts and 1 FPKM) and differentially expressed genes (> 2-fold) between IMR90 cells expressing shControl or shADAR1 as determined by the RNA-seq analysis.

c, Expression of SIRT1 mRNA was analyzed by RT-qPCR in the indicated IMR90 cells.

d, Heatmap of HuR-associated mRNAs that are significantly reduced by ADAR1 knockdown in IMR90 cells. List of 5 genes related to autophagy pathway was included in the top and the top 25 of the rest of genes identified were listed. IMR90 cells expressing shHuR were used as a positive control.

e-f, Expression of the indicated proteins was determined by immunoblot in the IMR90 cells expressing shControl or the indicated shHuR (**e**) and relative ADAR1 levels were quantified (**f**).

g, Immunoblot of HuR in IMR90 cells with the indicated treatment immunoprecipitated by an anti-HuR antibody. An isotype matched IgG was used as a negative control.

h, Expression of the indicated proteins was determined by immunoblot in the indicated IMR90 cells.

Data represent the mean ± s.d. in a and c and ± s.e.m. of three biologically independent experiments. *P* values were calculated using a two-tailed Student's *t*-test. Source numerical data and unprocessed blots are available in source data.

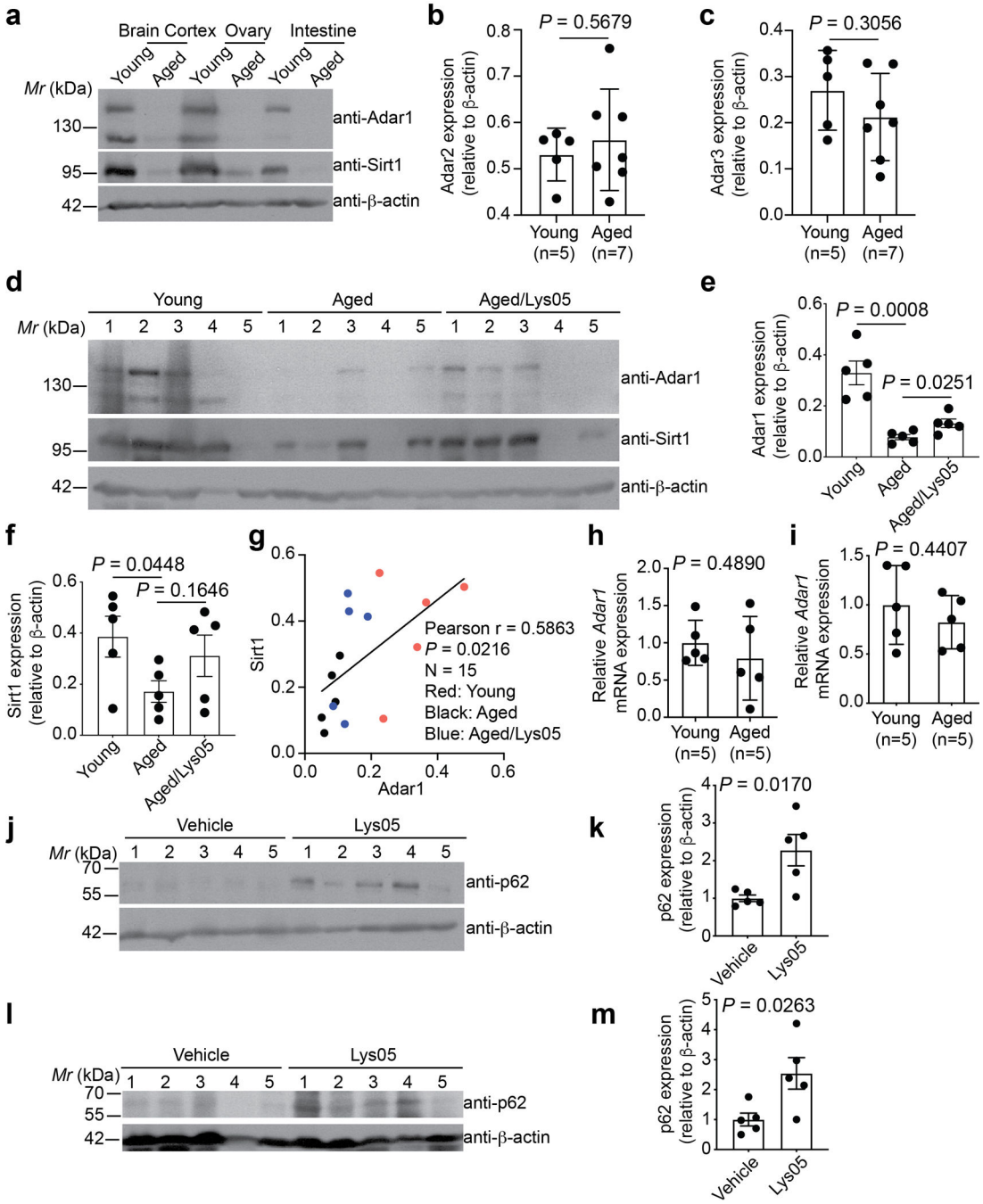

Extended Data Figure 5: Age-associated downregulation of Adar1

a, Expression of the indicated proteins was determined by immunoblot in the indicated tissues harvested from young (4 months) and aged (24 months) mice. The experiment was repeated two times independently with similar results.

b-c, The cortex tissues from brains of young (4 months) and aged (24 months) mice were analyzed for expression of the indicated proteins by immunoblot. The intensity of Adar2 (**b**) or Adar3 (**c**) immunoblot was quantified by NIH ImageJ software in young and aged mouse cortex tissues and normalized against a loading control β-actin expression.

d-g, Expression of Adar1 and Sirt1 was determined by immunoblot in the intestine tissues harvested from young mice (4 months), and aged mice (20 months) treated with either vehicle PBS control or Lys05 (10 mg/kg daily) for 2 weeks (**d**). The intensity of Adar1 (**e**) and Sirt1 (**f**) immunoblot was quantified using NIH ImageJ software in indicated groups by normalizing against a loading control β-actin expression. Correlation between Adar1 and Sirt1 protein expression as determined by a two-sided Pearson correlation analysis (**g**).
h-i, Expression of *Adar1* mRNA was analyzed by RT-qPCR in ovaries (h) and intestines (i) from young (4 months) and aged mice (20 months) treated with either vehicle PBS control or Lys05.
j-m, Expression of p62 was determined by immunoblot in ovaries (j) and intestines (l) from young mice (4 months) and aged mice (20 months) treated with either vehicle PBS control or Lys05. The intensity of p62 immunoblot in ovaries (k) and intestines (m) was quantified using NIH ImageJ software by normalizing against a loading control β-actin expression. Data represent the mean ± s.d. in b, c, e and f, or s.e.m. in h, I, k and m of biologically independent experiments. *P* values were calculated using a two-tailed Student's *t*-test. Source numerical data and unprocessed blots are available in source data.

Supplementary Material

Refer to Web version on PubMed Central for supplementary material.

Acknowledgement

We thank Dr. Chengyu Liang for critical reading of the manuscript and comments. This work was supported by US National Institutes of Health grants (R01CA160331 to R.Z., P01AG031862 to P.D.A., S.L.B and R.Z., R01GM040536 and R01GM130716 to K.N., and R50CA211199 to A.V.K.). K.N. was supported by a grant from Emerson Collective. Support of Core Facilities was provided by Cancer Centre Support Grant (CCSG) CA010815 to The Wistar Institute.

Data availability

RNA-seq datasets have been deposited in the Gene Expression Omnibus (GEO) under accession number: GSE179423. Source data have provided in Source Data. All other data supporting the findings of this study are available from the corresponding author on reasonable request.

References

1. Kim WY & Sharpless NE The regulation of INK4/ARF in cancer and aging. Cell 127, 265–275, doi:10.1016/j.cell.2006.10.003 (2006). [PubMed: 17055429]
2. Baker DJ et al. Clearance of p16Ink4a-positive senescent cells delays ageing-associated disorders. Nature 479, 232–236, doi:10.1038/nature10600 (2011). [PubMed: 22048312]
3. Deng P et al. Adar RNA editing-dependent and -independent effects are required for brain and innate immune functions in Drosophila. Nat Commun 11, 1580, doi:10.1038/s41467-020-15435-1 (2020). [PubMed: 32221286]
4. Sebastiani P et al. RNA editing genes associated with extreme old age in humans and with lifespan in C. elegans. PLoS One 4, e8210, doi:10.1371/journal.pone.0008210 (2009). [PubMed: 20011587]
5. Herranz N & Gil J Mechanisms and functions of cellular senescence. J Clin Invest 128, 1238–1246, doi:10.1172/JCI95148 (2018). [PubMed: 29608137]

6. He S & Sharpless NE Senescence in Health and Disease. Cell 169, 1000–1011, doi:10.1016/j.cell.2017.05.015 (2017). [PubMed: 28575665]
7. Bussian TJ et al. Clearance of senescent glial cells prevents tau-dependent pathology and cognitive decline. Nature 562, 578–582, doi:10.1038/s41586-018-0543-y (2018). [PubMed: 30232451]
8. Nishikura K Functions and regulation of RNA editing by ADAR deaminases. Annu Rev Biochem 79, 321–349, doi:10.1146/annurev-biochem-060208-105251 (2010). [PubMed: 20192758]
9. Nishikura K A-to-I editing of coding and non-coding RNAs by ADARs. Nat Rev Mol Cell Biol 17, 83–96, doi:10.1038/nrm.2015.4 (2016). [PubMed: 26648264]
10. Sakurai M et al. ADAR1 controls apoptosis of stressed cells by inhibiting Staufen1-mediated mRNA decay. Nat Struct Mol Biol 24, 534–543, doi:10.1038/nsmb.3403 (2017). [PubMed: 28436945]
11. Khan A et al. Membrane and synaptic defects leading to neurodegeneration in Adar mutant Drosophila are rescued by increased autophagy. BMC Biol 18, 15, doi:10.1186/s12915-020-0747-0 (2020). [PubMed: 32059717]
12. Amaravadi RK & Winkler JD Lys05: a new lysosomal autophagy inhibitor. Autophagy 8, 1383–1384, doi:10.4161/auto.20958 (2012). [PubMed: 22878685]
13. Dou Z et al. Autophagy mediates degradation of nuclear lamina. Nature 527, 105–109, doi:10.1038/nature15548 (2015). [PubMed: 26524528]
14. Xu C et al. SIRT1 is downregulated by autophagy in senescence and ageing. Nat Cell Biol 22, 1170–1179, doi:10.1038/s41556-020-00579-5 (2020). [PubMed: 32989246]
15. Pankiv S et al. p62/SQSTM1 binds directly to Atg8/LC3 to facilitate degradation of ubiquitinated protein aggregates by autophagy. J Biol Chem 282, 24131–24145, doi:10.1074/jbc.M702824200 (2007). [PubMed: 17580304]
16. Narita M et al. Rb-mediated heterochromatin formation and silencing of E2F target genes during cellular senescence. Cell 113, 703–716, doi:10.1016/s0092-8674(03)00401-x (2003). [PubMed: 12809602]
17. Zhang R et al. Formation of MacroH2A-containing senescence-associated heterochromatin foci and senescence driven by ASF1a and HIRA. Dev Cell 8, 19–30, doi:10.1016/j.devcel.2004.10.019 (2005). [PubMed: 15621527]
18. Lai F, Drakas R & Nishikura K Mutagenic analysis of double-stranded RNA adenosine deaminase, a candidate enzyme for RNA editing of glutamate-gated ion channel transcripts. J Biol Chem 270, 17098–17105, doi:10.1074/jbc.270.29.17098 (1995). [PubMed: 7615504]
19. Martin N, Beach D & Gil J Ageing as developmental decay: insights from p16(INK4a.). Trends Mol Med 20, 667–674, doi:10.1016/j.molmed.2014.09.008 (2014). [PubMed: 25277993]
20. Huang J et al. SIRT1 overexpression antagonizes cellular senescence with activated ERK/S6k1 signaling in human diploid fibroblasts. PLoS One 3, e1710, doi:10.1371/journal.pone.0001710 (2008). [PubMed: 18320031]
21. Li Y & Tollefsbol TO p16(INK4a) suppression by glucose restriction contributes to human cellular lifespan extension through SIRT1-mediated epigenetic and genetic mechanisms. PLoS One 6, e17421, doi:10.1371/journal.pone.0017421 (2011). [PubMed: 21390332]
22. Wang IX et al. ADAR regulates RNA editing, transcript stability, and gene expression. Cell Rep 5, 849–860, doi:10.1016/j.celrep.2013.10.002 (2013). [PubMed: 24183664]
23. Fan XC & Steitz JA Overexpression of HuR, a nuclear-cytoplasmic shuttling protein, increases the in vivo stability of ARE-containing mRNAs. EMBO J 17, 3448–3460, doi:10.1093/emboj/17.12.3448 (1998). [PubMed: 9628880]
24. Zhang Z et al. Activation of ferritinophagy is required for the RNA-binding protein ELAVL1/HuR to regulate ferroptosis in hepatic stellate cells. Autophagy 14, 2083–2103, doi:10.1080/15548627.2018.1503146 (2018). [PubMed: 30081711]
25. Levine B & Kroemer G Autophagy in the pathogenesis of disease. Cell 132, 27–42, doi:10.1016/j.cell.2007.12.018 (2008). [PubMed: 18191218]
26. Fernandez AF et al. Disruption of the beclin 1-BCL2 autophagy regulatory complex promotes longevity in mice. Nature 558, 136–140, doi:10.1038/s41586-018-0162-7 (2018). [PubMed: 29849149]

27. Lin SJ, Defossez PA & Guarente L Requirement of NAD and SIR2 for life-span extension by calorie restriction in Saccharomyces cerevisiae. Science 289, 2126–2128, doi:10.1126/science.289.5487.2126 (2000). [PubMed: 11000115]
28. Tissenbaum HA & Guarente L Increased dosage of a sir-2 gene extends lifespan in Caenorhabditis elegans. Nature 410, 227–230, doi:10.1038/35065638 (2001). [PubMed: 11242085]
29. Rogina B & Helfand SL Sir2 mediates longevity in the fly through a pathway related to calorie restriction. Proc Natl Acad Sci U S A 101, 15998–16003, doi:10.1073/pnas.0404184101 (2004). [PubMed: 15520384]

References

30. Dou Z et al. Cytoplasmic chromatin triggers inflammation in senescence and cancer. Nature 550, 402–406, doi:10.1038/nature24050 (2017). [PubMed: 28976970]
31. Zhang R, Chen W & Adams PD Molecular dissection of formation of senescence-associated heterochromatin foci. Mol Cell Biol 27, 2343–2358, doi:10.1128/MCB.02019-06 (2007). [PubMed: 17242207]
32. Mitra M, Ho LD & Coller HA An In Vitro Model of Cellular Quiescence in Primary Human Dermal Fibroblasts. Methods Mol Biol 1686, 27–47, doi:10.1007/978-1-4939-7371-2_2 (2018). [PubMed: 29030810]
33. Hari P et al. The innate immune sensor Toll-like receptor 2 controls the senescence-associated secretory phenotype. Sci Adv 5, eaaw0254, doi:10.1126/sciadv.aaw0254 (2019). [PubMed: 31183403]
34. Liu P et al. m(6)A-independent genome-wide METTL3 and METTL14 redistribution drives the senescence-associated secretory phenotype. Nat Cell Biol 23, 355–365, doi:10.1038/s41556-021-00656-3 (2021). [PubMed: 33795874]
35. Cheng LC et al. Alternative 3' UTRs play a widespread role in translation-independent mRNA association with the endoplasmic reticulum. Cell Rep 36, 109407, doi:10.1016/j.celrep.2021.109407 (2021). [PubMed: 34289366]
36. Weng H et al. METTL14 Inhibits Hematopoietic Stem/Progenitor Differentiation and Promotes Leukemogenesis via mRNA m(6)A Modification. Cell Stem Cell 22, 191–205 e199, doi:10.1016/j.stem.2017.11.016 (2018). [PubMed: 29290617]
37. Langmead B & Salzberg SL Fast gapped-read alignment with Bowtie 2. Nat Methods 9, 357–359, doi:10.1038/nmeth.1923 (2012). [PubMed: 22388286]
38. Li B & Dewey CN RSEM: accurate transcript quantification from RNA-Seq data with or without a reference genome. BMC Bioinformatics 12, 323, doi:10.1186/1471-2105-12-323 (2011). [PubMed: 21816040]
39. Love MI, Huber W & Anders S Moderated estimation of fold change and dispersion for RNA-seq data with DESeq2. Genome Biol 15, 550, doi:10.1186/s13059-014-0550-8 (2014). [PubMed: 25516281]
40. Koboldt DC et al. VarScan 2: somatic mutation and copy number alteration discovery in cancer by exome sequencing. Genome Res 22, 568–576, doi:10.1101/gr.129684.111 (2012). [PubMed: 22300766]
41. Kang TW et al. Senescence surveillance of pre-malignant hepatocytes limits liver cancer development. Nature 479, 547–551, doi:10.1038/nature10599 (2011). [PubMed: 22080947]

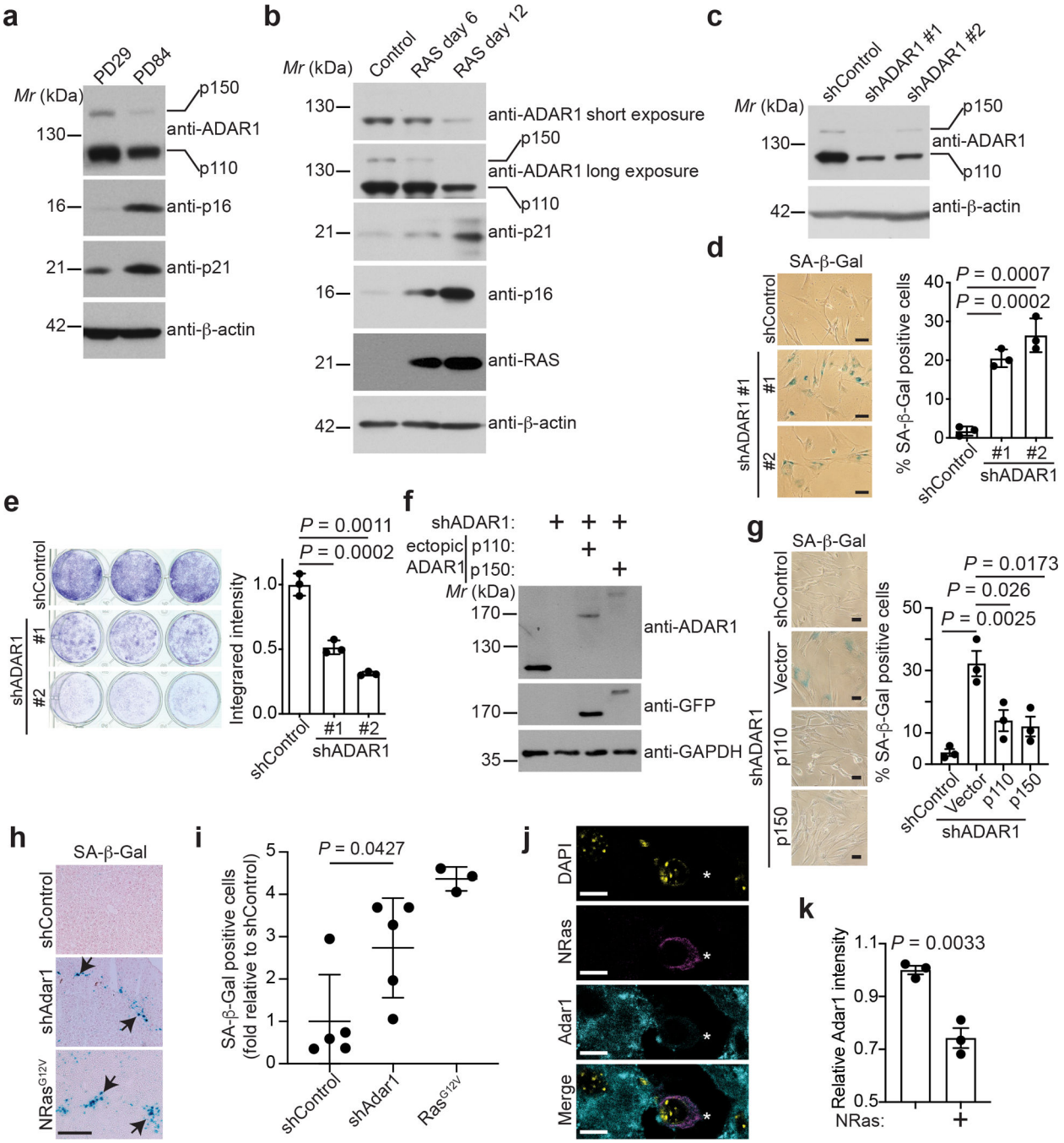

Figure 1: ADAR1 downregulation drives senescence.

a, IMR90 cells at the indicated passage double (PD) were harvested and analyzed for expression of the indicated proteins by immunoblot. The experiment was repeated three times independently with similar results.

b, IMR90 cells were infected with retrovirus encoding oncogenic H-RAS^{G12V} to induce senescence. Cells were harvested at the indicated timepoints to analyze for the expression of the indicated proteins by immunoblot. The experiment was repeated three times independently with similar results.

c-e, IMR90 cells infected with the indicated shRNAs were analyzed for expression of the indicated proteins by immunoblot (**c**) or stained for SA-β-gal activity and quantified for percentage of positive cells (**d**). In addition, the indicated cells were subjected to colony formation assay and the intensity of colonies formed by the indicated cells were quantified (**e**). Scale bars = 100 μm.

f-g, IMR90 cells expressing shControl or shADAR1 (#1) with or without ectopic ADAR1p110 and ADAR1p150 restoration were analyzed for expression of the indicated proteins by immunoblot (**f**) or stained for SA-β-Gal activity and quantified for percentage of positive cells (**g**). Scale bars = 100 μm.

h-i, Representative images of SA-β-gal staining of mouse liver from the indicated groups at day 6 post injection (**h**), and the number of SA-β-gal-positive cells in the indicated groups (n=5 biologically independent mice in shControl and shAdar1 expressing group and n=3 mice for $NRas^{G12V}$ group). Scale bars = 100 μm.

j-k, Immunostaining for NRas and Adar1 in mouse liver from $NRas^{G12V}$-expressing group in the hydrodynamic tail vein injection model. DAPI counter staining was used to visualize the nuclei. Asterisks indicated examples of decreased level of Adar1 in $NRas^{G12V}$-expressing senescent hepatocyte (**j**) and relative Adar1 intensity was quantified (**k**). (n=3 biologically independent mice). Scale bars = 10 μm. Data represents the mean ± s.d. in d, e and i, or s.e.m. in k of three biologically independent experiments. Source numerical data and unprocessed blots are available in source data.

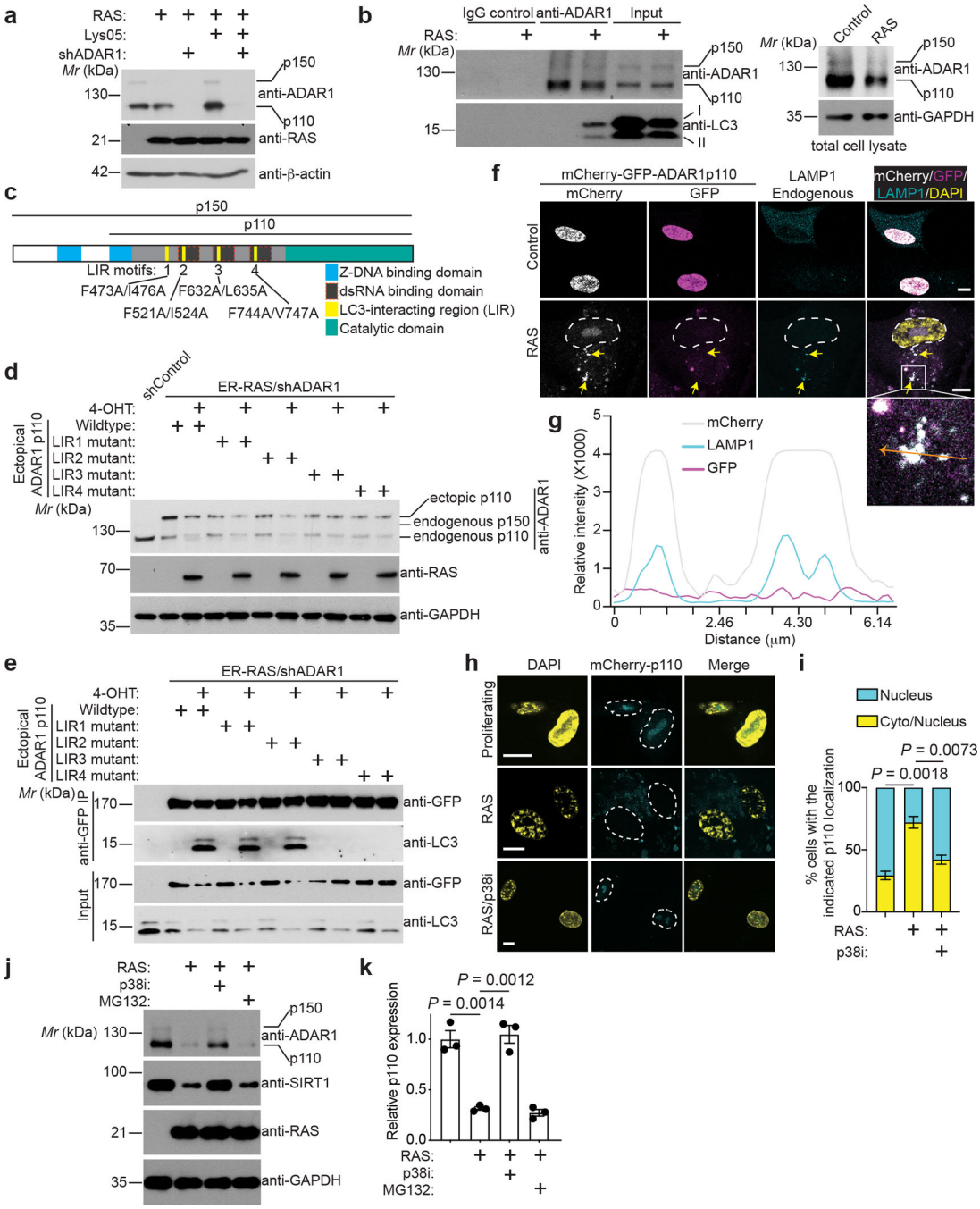

Figure 2: Autophagy-dependent downregulation of ADAR1 during senescence.

a, The indicated IMR90 cells were treated with or without Lys05 and analyzed for expression of the indicated proteins. The experiment was repeated three times independently with similar results.

b, Co-immunoprecipitation analysis between ADAR1 and LC3 in cytoplasmic extracts from the indicated IMR90 cells. The experiment was repeated three times independently with similar results.

c, Scheme of ADAR1 showing the location of four LC3-interacting region (LIR) motifs.

d-e, Co-immunoprecipitation analysis was performed between ectopic ADAR1 and LC3 in ER:RAS-expressing IMR90 cells with endogenous ADAR1 knockdown and expression of mCherry-GFP tagged ectopic wildtype or the LIR motif mutant ADAR1 with or without RAS induction (**d**). In addition, expression of ectopically expressed ADAR1 wildtype or mutants was examined by immunoblot using an anti-ADAR1 antibody (**e**). The experiment was repeated three times independently with similar results. Note that shADAR1 #1 does not target ectopic ADAR1 because shADAR1 targets 3' UTR region.

f-g, Immunostaining for LAMP1 in IMR90 cells expressing mCherry-GFP-ADAR1p110 with or without RAS induction. The arrows indicate examples of cytoplasmic ADAR1 puncta with strong mCherry and faded GFP signal, indicating the localization of ADAR1 in acidic (auto)lysosomes (**f**). The relative intensities of the mCherry, GFP and LAMP1 signals of a typical senescent cell as in **f** were quantified (**g**). Dash lines indicate nuclei. Scale bars = 10 μm. The experiment was repeated three times independently with similar results.

h-i, IMR90 cells transfected with mCherry-ADAR1 p110 were induced to senescence by expressing RAS, and treated with or without p38 inhibitor SB203580. Localization of mCherry-ADAR1p110 was visualized (**h**), and the indicated distribution pattern was quantified (**i**). Dash lines indicate nuclei. Scale bars = 10 μm.

j-k, Immunoblot of the indicated proteins in IMR90 cells expressing RAS, and treated with or without p38i SB203580 or MG132 (**j**). And the relative expression of ADAR1p110 was quantified (**k**).

Data represents the mean ± s.e.m. in i and k of three biologically independent experiments. *P* values were calculated using a two-tailed Student's *t*-test. Source numerical data and unprocessed blots are available in source data.

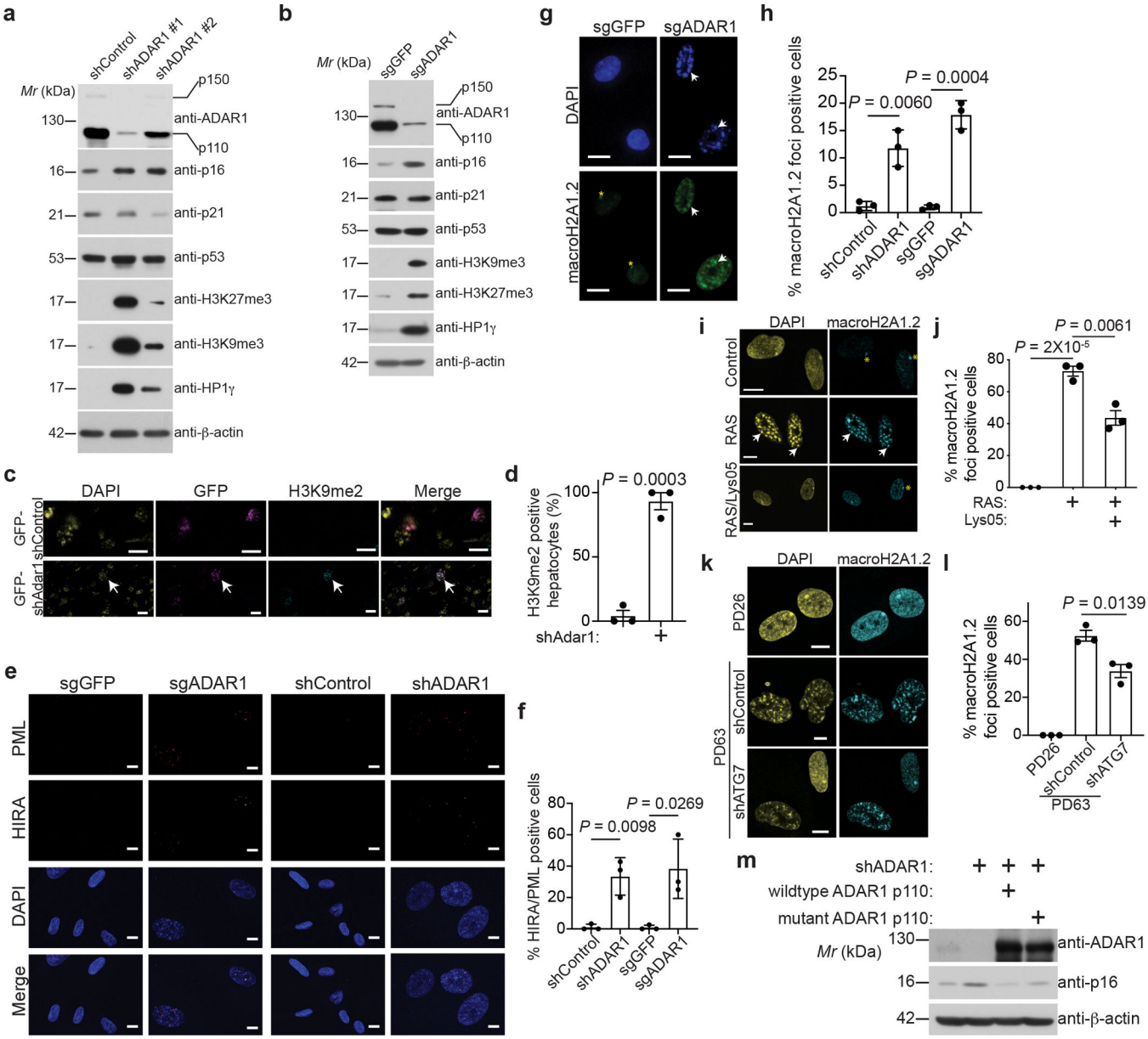

Figure 3: ADAR1 loss promotes heterochromatin formation independent of its RNA editing function

a, IMR90 cells expressing indicated shRNAs were analyzed for expression of the indicated proteins. The experiment was repeated three times independently with similar results.

b, IMR90 cells expressing the indicated sgRNAs were analyzed for expression of the indicated proteins. The experiment was repeated three times independently with similar results.

c-d, Immunostaining for H3K9me2 in mouse livers from indicated groups in the hydrodynamic tail vein injection model (**c**), which was quantified (**d**) from three biologically independent mice. The arrow indicates an example of clusters of shAdar1-expressing hepatocytes with an increase in H3K9me2 levels.

e-f, Immunostaining for HIRA and PML in the indicated IMR90 cells (**d**), and the percentage of HIRA/PML foci positive cells were quantified (> 200 cells) (**e**).
g-h, Immunostaining for macroH2A1.2 in IMR90 cells expressing the indicated sgRNAs (**f**), and the percentage of macroH2A1.2 foci positive cells were quantified (> 200 cells) (**g**). Asterisks indicated inactivated X chromosome in female IMR90 cells and arrows point examples of macroH2A1.2 positive SAHF.
i-j, Immunostaining for macroH2A1.2 in control and RAS-induced senescent IMR90 cells with and without Lys05 treatment (**i**), and the percentage of macroH2A1.2 foci positive cells were quantified (> 200 cells) (**j**).
k-l, Immunostaining for macroH2A1.2 in proliferating (PD26) and replicative senescent (PD63) IMR90 cells with and without ATG7 knockdown (**k**), and the percentage of macroH2A1.2 foci positive cells were quantified (> 200 cells) (**l**).
m, IMR90 cells expressing shControl or shADAR1 (#1) with or without rescue by ectopically expression of wildtype ADAR1 p110 or a deaminase inactive mutant E912A ADAR1 p110 were analyzed for expression of the indicated proteins. The experiment was repeated three times independently with similar results.
Data represent the mean ± s.d. in f and h, or s.e.m. in d, j and l of three biologically independent experiments. Scale bars = 10 μm. *P* values were calculated using a two-tailed Student's *t*-test. Source numerical data and unprocessed blots are available in source data.

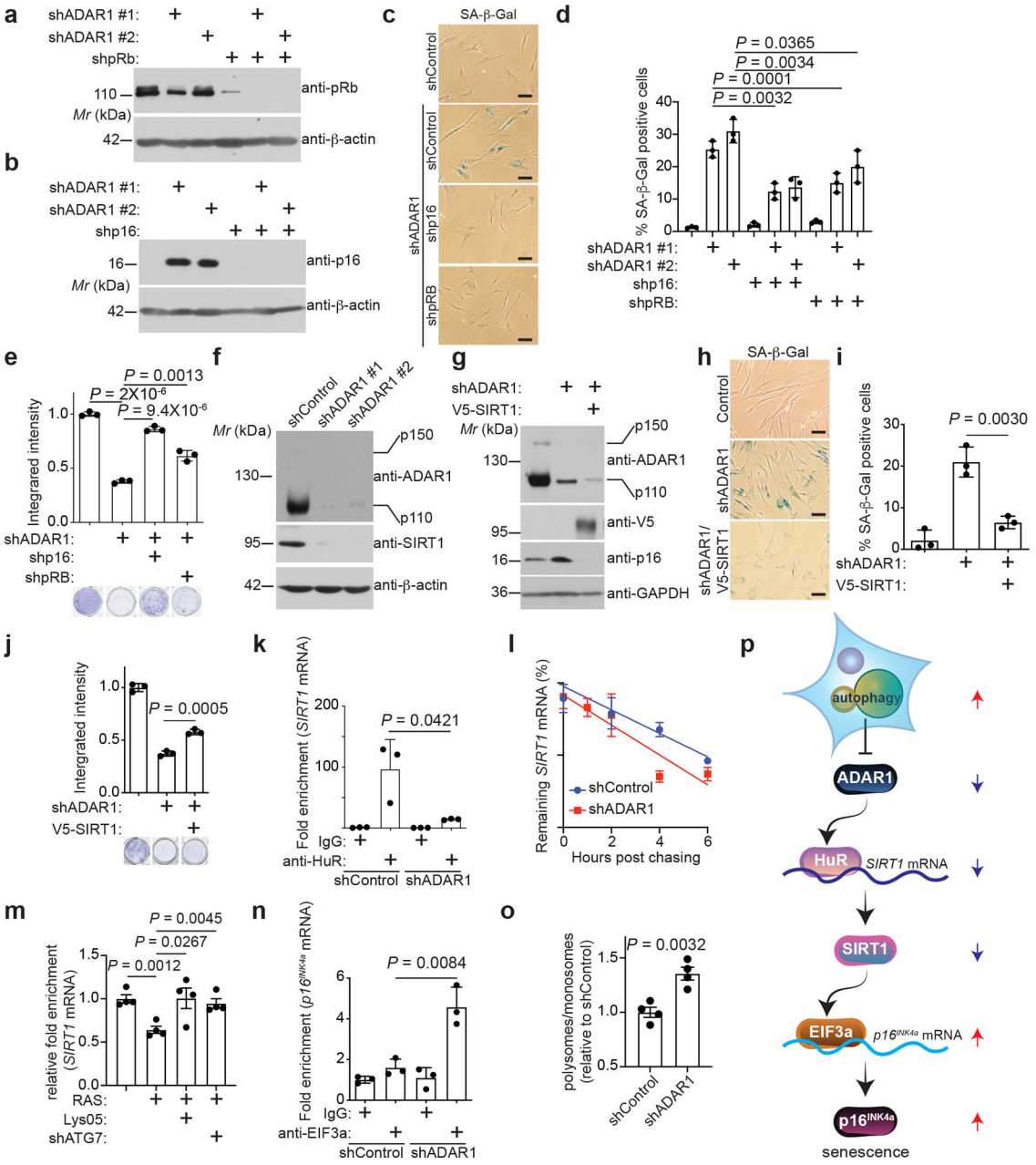

Figure 4: ADAR1 loss promotes senescence by upregulating p16^{INK4a} via SIRT1

a-e, IMR90 cells expressing shControl or shADAR1 with or without simultaneous shpRb (**a**) or shp16^{INK4a} (**b**) expression were analyzed for expression of the indicated proteins or stained for SA-β-Gal activity (**c**). Percentage of SA-β-Gal positive cells were quantified (> 200 cells) (**d**). The indicated cells were subjected to colony formation assay to determine senescence-associated growth arrest (**e**). Scale bars = 100 μm. The experiment was repeated three times independently with similar results.

f, IMR90 cells expressing shControl or shADAR1s were analyzed for expression of the indicated proteins. The experiment was repeated three times independently with similar results.

g-j, IMR90 cells expressing shControl or shADAR1 (#1) with or without ectopic V5-tagged SIRT1 expression were analyzed for expression of the indicated proteins (**g**). The indicated cells were stained for SA-β-Gal activity (**h**) and positive cells were quantified (> 200 cells) (**i**). The indicated cells were also subjected to colony formation (**j**). Scale bars = 100 μm.
k-l, IMR90 cells expressing shControl or shADAR1 (#1) were subjected to RNA immunoprecipitation analysis using an anti-HuR antibody for *SIRT1* mRNA (**k**), or treated with actinomycin D and chased for 2, 4 and 6 hours and expression of SIRT1 mRNA was determined by RT-qPCR (**l**).
m, The indicated IMR90 cells were subjected to RNA immunoprecipitation analysis using an anti-HuR antibody for *SIRT1* mRNA.
n, IMR90 cells expressing shControl or shADAR1 (#1) were subjected to RNA immunoprecipitation analysis using an anti-ELF3a antibody for $p16^{INK4a}$ mRNA.
o, Polysome profiling assay was performed in IMR90 cells with or without ADAR1 knockdown. The association of $p16^{INK4a}$ mRNA with polysomes or monosomes was quantified using RT-qPCR. The experiment was repeated two times with similar results.
p, A model on how autophagy-mediated ADAR1 downregulation promotes senescence via upregulating $p16^{INK4a}$ through SIRT1 post-transcriptionally.
Data represent the mean ± s.d. in d, e, i, j, k, l and n, or s.e.m. in m and o of three biologically independent experiments unless otherwise stated. *P* values were calculated using a two-tailed Student's *t*-test. Source numerical data and unprocessed blots are available in source data.

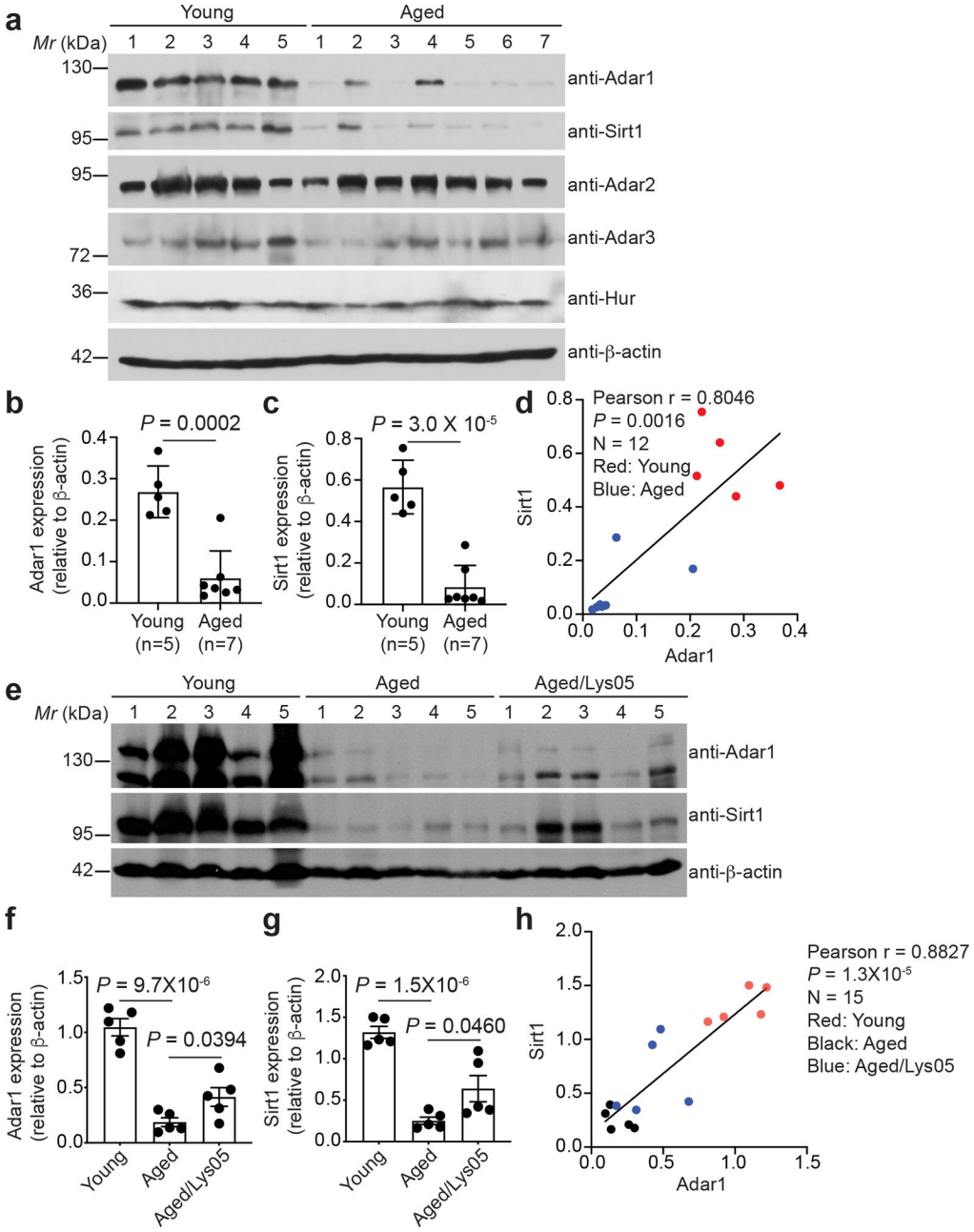

Figure 5: Inhibition of lysosomal pathway reverses age-associated decline in ADAR1 expression

a-c, The cortex tissues from brains of young (4 months) and aged (24 months) mice were analyzed for expression of the indicated proteins by immunoblot (**a**). The intensity of Adar1 (**b**) and Sirt1 (**c**) immunoblot was quantified by NIH ImageJ software in young and aged mouse cortex tissues and normalized against a loading control β-actin expression. Correlation between Adar1 and Sirt1 protein expression was determined by Pearson correlation analysis (**d**).

e-h, Expression of Adar1 and Sirt1 was determined by immunoblot in the ovary tissues harvested from young mice (4 months), and aged mice (20 months) treated with vehicle PBS control or Lys05 (10 mg/kg daily) for 2 weeks (**e**). The intensity of Adar1 (**f**) and Sirt1 (**g**)

immunoblot was quantified by NIH ImageJ software in indicated groups and normalized against a loading control β-actin expression. Correlation between Adar1 and Sirt1 protein expression was determined by a two-sided Pearson correlation analysis (**h**). n=5 biologically independent mice per group.

Data represent the mean ± s.d. in b and c, or s.e.m. in f and g of biologically independent experiments. *P* values were calculated using a two-tailed Student's *t*-test in b, c, f and g, or a two-sided Pearson correlation analysis in d and h. Source numerical data and unprocessed blots are available in source data.